UNIVERSIDADE FEDERAL DE ITAJUBÁ

PROGRAMA DE PÓS-GRADUAÇÃO EM
ENGENHARIA DE PRODUÇÃO

Juliana Helena Daroz Gaudêncio

Otimização multiobjetivo por estimadores robustos multivariados

Itajubá, 2019

UNIVERSIDADE FEDERAL DE ITAJUBÁ

PROGRAMA DE PÓS-GRADUAÇÃO EM
ENGENHARIA DE PRODUÇÃO

Juliana Helena Daroz Gaudêncio

Otimização multiobjetivo por estimadores robustos multivariados

Tese submetida ao Programa de Pós-Graduação em Engenharia de Produção como parte dos requisitos para obtenção do título de **Doutor em Ciências em Engenharia de Produção**.

Área de Concentração: Modelagem e Otimização
Orientador: Prof. João Batista Turrioni, Dr.
Coorientador: Prof. Anderson Paulo de Paiva, Dr.

Itajubá, 2019

UNIVERSIDADE FEDERAL DE ITAJUBÁ

PROGRAMA DE PÓS-GRADUAÇÃO EM
ENGENHARIA DE PRODUÇÃO

Juliana Helena Daroz Gaudêncio

Otimização multiobjetivo por estimadores robustos multivariados

Tese aprovada por banca examinadora em 25 de fevereiro de 2019, conferindo ao autor o título de **Doutor em Ciências em Engenharia de Produção**.

Banca Examinadora:

Prof. Dr. João Batista Turrioni (Orientador)

Prof. Dr. Anderson Paulo de Paiva (Co-orientador)

Prof. Dr. Pedro Paulo Balestrassi (UNIFEI)

Prof. Dr. Rafael Coradi Leme (UNIFEI)

Prof. Dr. Roberto da Costa Quinino (UFMG)

Prof. Dr. Rogério Santana Peruchi (UFPB)

Itajubá, 2019

DEDICATÓRIA

Ao meu marido, Thiago, que sempre me incentivou e esteve presente no desenvolvimento deste trabalho.

AGRADECIMENTOS

Ao meu orientador, João Batista Turrioni e, ao meu coorientador, Anderson Paulo de Paiva, pela disponibilidade que sempre tiveram em me orientar, pelas importantes contribuições no desenvolvimento da pesquisa e, principalmente, pela confiança que depositaram no meu trabalho. Aos demais professores do Instituto de Engenharia de Produção e Gestão da UNIFEI que serem estiveram dispostos a me ajudar, sobretudo com o conhecimento adquirido ao longo da minha trajetória na pós-graduação.

À minha família pelo carinho e amor incondicional ao longo de toda a trajetória. Meus pais, Jorge e Maria Vilma, meus irmãos, Vitor e Laura. Em especial, ao meu marido, Thiago, que sempre me acompanhou, incentivando e dividindo os momentos de conquista.

Aos colegas do GEPE de Qualidade pelo companheirismo e por fazerem a jornada mais prazerosa e a todos os meus amigos que contribuíram direta ou indiretamente para essa conquista.

A CAPES pelo apoio financeiro concedido para a realização deste trabalho através do programa de bolsa de estudos.

“A verdadeira viagem de descobrimento não consiste em procurar novas paisagens,
mas em ter novos olhos.”
Marcel Proust

RESUMO

As organizações focam em determinar condições ideais de operação com o intuito de garantir a qualidade de seus processos e serviços, uma vez que os processos industriais podem exibir um elevado grau de variabilidade. Neste contexto, o uso de estimadores robustos torna-se uma alternativa adequada para modelar os dados experimentais; sendo que o termo robusto descreve a capacidade que um estimador tem em superar as influências exercidas pelos valores discrepantes. Encontrar uma combinação de estimadores de centralidade e dispersão que seja capaz de modelar dados suscetíveis à variabilidade é um desafio a ser explorado. Desse modo, este presente trabalho, com o auxílio da Análise de Componentes Principais (ACP), visa à obtenção de respostas transformadas em escores de componentes que explicarão a estrutura de variância-covariância a partir de combinações lineares das varáveis originais. Em consequência, o objetivo geral é o de validar um algoritmo de otimização multiobjetivo baseado no agrupamento de respostas correlacionadas e modeladas por estimadores robustos. Com o auxílio do método da Interseção Normal à Fronteira, é proposta uma otimização multiobjetivo para funções obtidas pelo Erro Quadrático Médio Multivariado (EQMM) que combina técnicas da Metodologia de Superfície de Resposta com a ACP, visando obter soluções Pareto-ótimas. O objeto de estudo definido para a aplicação desta proposta é o processo de torneamento do aço de corte fácil ABNT/SAE 12L14 composto por um arranjo cruzando onde 12 condições de ruído são consideradas para a obtenção da variável de resposta que é a rugosidade superficial (R_a). O resultado ótimo é definido pelo tomador de decisão fuzzy e para provar a eficiência da resposta encontrada, experimentos de confirmação foram realizados. Em um nível de confiança de 95%, o valor ótimo pertence aos intervalos de confiança multivariados apenas para o Modelo B, no qual a mediana e o MAD são considerados e, confirmando assim, qual par de estimadores atinge a solução em um cenário de projeto robusto de parâmetro. Através da pesquisa proposta, o modelo desenvolvido pode ser utilizado em indústrias para determinação de parâmetros de usinagem para obtenção de alta qualidade com consumo mínimo de energia e, consequentemente, máxima produtividade.

Palavras-Chaves: Estimadores robustos; Correlação; Componentes Principais; Interseção Normal à Fronteira; Otimização Multiobjetivo.

ABSTRACT

Organizations focus on determining optimal operating conditions to ensure quality; however, industrial processes may exhibit high degree of variability. The use of robust estimators is a suitable alternative to model the experimental data since the term robust describes the ability of an estimator has to overcome the influences exerted by outliers. It is a challenge to be explored to find a combination of centrality and dispersion estimators that is capable of modeling data susceptible to variability. Thereby, this work aims to obtain transformed responses to principal components' scores that will explain the variance-covariance structure from linear combinations of the original variables. As a consequence, the main objective is to validate a multiobjective optimization algorithm based on the grouping of correlated responses and modeled by robust estimators. Further, with the assistance of Normal Boundary Intersection method, a multiobjective optimization is proposed considering functions obtained by the Multivariate Mean Square Error (MMSE) which combines techniques of the Response Surface Methodology with Principal Component Analysis in order to obtain Pareto-optimal solutions. As a case study, the surface roughness (R_a) of an AISI 12L14 steel turning process composed of a crossed array where there is 12 noise conditions is defined for this proposal. The method uses a fuzzy decision maker to show the surface roughness' optimum result with the most efficient production taken into consideration. To prove its efficiency, confirmation runs were conducted. At a confidence level of 95%, the optimal value falls within the multivariate confidence intervals only for Model B, in which the estimators' median and MAD are considered, thus affirming which pair of estimators achieves the most robust parameter design solution. Through the proposed research, the developed model can be used in industries for determining machining parameters to attain high quality with minimum power consumption and hence maximum productivity.

Keywords: Robust estimators; Correlation; Principal Components; Normal Boundary Intersection; Multiobjective Optimization.

LISTA DE FIGURAS

LISTA DE TABELAS

LISTA DE ABREVIATURAS E SIGLAS

ABNT	Associação Brasileira de Normas Técnicas
ACP	Análise de Componentes Principais
AHL	*Arc Homotopy Length*
EQMM	Erro Quadrático Médio Multivariado
GRG	*Generalized Reduced Gradient* / Gradiente Reduzido Generalizado
MAD	*Median Absolute Deviation*
MLE	*Maximum Likelihood Estimator*
MMSE	*Multivariate Mean Square Error*
NBI	*Normal Boundary Intersection*
NNC	*Normalized Normal Constraint*
PRP	Projeto Robusto de Parâmetro

SUMÁRIO

PREFÁCIO

O formato desta tese de doutorado seguiu a norma dos Programas de Pós Graduação da Universidade Federal de Itajubá (UNIFEI) aprovada na 18ª Reunião Ordinária (95ª Resolução) pelo CEPEAd (Conselho de Ensino, Pesquisa, Extensão e Administração) em 04/07/2018.

A seguir está descrito o Artigo 52 da **Subseção III – Do Formato da Tese**:

Art. 52. O formato da tese de doutorado será definido no Regulamento interno de cada PPG, podendo ser escrito no formato tradicional ou no formato de artigos, no idioma português ou inglês.

§1º. A tese em formato tradicional deve conter os elementos pré-textuais e pós-textuais (Referências, Apêndices e Anexos sendo os dois últimos opcionais), além de:

I. Introdução, Objetivos (pode constar na Introdução), Revisão da literatura (pode constar na Introdução), Metodologia ou Material e Métodos, Resultados e Discussão, Conclusão; ou

II. Introdução, Desenvolvimento e Conclusões.

§2º. A Tese de Doutorado no formato de artigos contempla a apresentação de no mínimo 3 (três) artigos resultantes, sendo pelo menos 1 (um) deles publicado ou com aceite formal (conforme §3º deste artigo) de um periódico de circulação internacional e os demais submetidos a periódicos, além dos elementos pré-textuais, um capítulo introdutório e um capítulo de conclusões sendo todos os itens descritos escritos em inglês.

§3º. O artigo publicado ou com aceite formal deve ser oriundo do trabalho de tese e ter qualidade reconhecida pela comunidade acadêmica da sua área de concentração, com circulação internacional, orientado pela classificação Qualis A2 ou superior (ou fator de impacto equivalente) do Comitê de Área de Avaliação do PPG na CAPES.

§4º. A defesa da tese no formato de artigos deve considerar apenas artigos onde o discente é o 1º autor (exceto para áreas que utilizam ordem alfabética para listagem dos autores) e deve conter a participação do orientador como coautor.

1. INTRODUÇÃO

1.1 Contexto da pesquisa

Partindo da pesquisa realizada em Gaudêncio (2015), cenários em que os processos de manufatura são inerentes à presença de ruídos podem proporcionar a não normalidade do conjunto de dados. Desse modo, surge à oportunidade de se trabalhar com estimadores robustos não paramétricos que são benéficos quando não se pode supor, previamente, a distribuição de probabilidade que melhor se adequa aos dados.

Neste contexto, processos que possuem mínima variação na presença de ruídos são denominados Projetos Robustos de Parâmetros (PRP), do inglês *Robust Parameter Design* que, segundo Ardakani e Noorossana (2008), trata-se de um conjunto de técnicas utilizadas com o intuito de aumentar a robustez do processo. Desta forma, o PRP almeja uma combinação de fatores controláveis visando que a medida de centralidade dos dados seja a mais próxima possível do seu valor alvo e que a medida de dispersão seja a menor possível assim, proporcionando a insensibilidade à ação dos ruídos.

Introduzida, inicialmente, por Genichi Taguchi, essa abordagem de análise e otimização da metodologia RPD vem sendo detalhado na literatura. Esses esforços de melhoria se concentraram na abordagem da superfície de resposta dual que foi incorporada na metodologia PRP por Vining e Myers (1990) conforme descrito em Elsayed e Lacor (2014).

Problemas envolvendo, ao mesmo tempo, o estudo de centralidade e dispersão dos dados, são denominados de problemas duais e, consequentemente, a média e a variância são os estimadores mais comumente utilizados, mas, conforme já exposto, os processos industriais exibem uma elevada variabilidade que acarretam em observações altamente variáveis em decorrência dos ruídos de processo. Desse modo, os estimadores robustos de localização e escala surgem como uma alternativa por possuírem a capacidade de modelar tais observações extremas sem ter que retirá-las da amostra (BOYLAN e CHO (2013)).

A partir desta proposta apresentada em Gaudêncio (2015), foram expostas alternativas para a modelagem da centralidade e dispersão dos dados através de cinco estimadores robustos de localização e seis estimadores robustos de escala conforme listados na Tabela 1. O termo robusto descreve a capacidade que um estimador tem de superar as influências exercidas pelos dados extremos (*outliers*).

Tabela 1 – Pares de estimadores paramétricos e não paramétricos

Modelo	**Estimadores de localização**	**Estimadores de escala**
A	Média $(\bar{x})$	Desvio-padrão (s)
B	Mediana $(\tilde{x})$	Median absolute deviation (MAD)
C	Huber's Proposal 2 $(\tilde{x}_{H2})$	Huber's Proposal 2 (S_{H2})
D	Hodges–Lehmann estimator (HL_n)	S_n estimator
E	Hodges–Lehmann estimator (HL_n)	Q_n estimator
F	Tau $(\tilde{x}_\tau)$	Tau (s_τ)
G	Hodges–Lehmann estimator (HL_n)	Median absolute deviation (MAD)
H	Maximum likelihood estimator $(\tilde{x}_{MLE})$	Maximum likelihood estimator (s_{MLE})

Fonte: Adaptado de Boylan e Cho (2013)

O uso de estimadores robustos também é reforçado no trabalho de Park e Cho (2003) que menciona que os estimadores mais populares dos parâmetros de localização e escala são, respectivamente, a média e a variância, mas sendo estes muito sensíveis à presença de *outliers* que, por sua vez, podem apresentar valores inesperados em relação a maior parte da amostra. Portanto, há situações práticas em que a média da amostra e a variância precisam ser substituídas por estimadores que são menos sensíveis a presença de valores extremos. Conforme detalhado em Hampel *et al*. (1986), existem muitas classes de estimadores robustos; os mais tradicionais são os estimadores-L (combinações lineares de observações de ordem), estimadores-M (generalizações de um estimador de máxima verossimilhança) e os estimadores-R (estimador baseado no ranqueamento dos resíduos).

Os estimadores apresentados na Tabela 1 são considerados potenciais alternativas para a média da amostra e para a variância e foram selecionados por Boylan e Cho (2013) por duas razões: (1) a média e a variância são os estimadores mais comuns utilizados na camada inicial de estimação e, também, já foram examinados em ambientes PRP e, assim, fornecendo uma base lógica de comparação para os dados que serão examinados e (2) os demais estimadores são bem conhecidos no campo da estatística devido a robustez e eficiência que eles apresentam, mas ainda não foram testados em ambientes PRP, por isso, são considerados potenciais alternativas. Além disso, esses estimadores não paramétricos possuem notável classificação nas propriedades de eficiência relativa e ponto de ruptura.

O ponto de ruptura de uma amostra finita é a fração máxima de *outliers* que podem ser adicionados em uma dada amostra, sem prejudicar a estimativa por completo e não pode exceder o valor de 50%, pois se mais da metade das observações estão contaminadas, não é possível distinguir entre a distribuição subjacente e a distribuição contaminada (YOHAI e ZAMAR, 1988). Já a eficiência relativa é atribuída em relação à distribuição normal, ou seja, quando um estimador robusto for utilizado em dados normalmente distribuídos, quanto menor

a sua eficiência relativa, piores serão os resultados produzidos em relação aos obtidos por meio da média e do desvio padrão (SERFLING, 2011).

Assim sendo, a modelagem realizada pelos estimadores descritos na Tabela 1 proporcionou vários cenários de otimização promovendo um ranqueamento para fins de comparação de desempenho.

1.2 Justificativa do trabalho

As respostas otimizadas pelo Método da Interseção Normal à Fronteira, do inglês *Normal Boundary Intersection* (NBI), proposto por Das e Dennis (1998), originaram fronteiras de Pareto com eixos correlacionados (centralidade x dispersão) e, assim, dificultando a obtenção de fronteiras convexas e equiespaçadas. A dificuldade de se otimizar respostas correlacionadas pelo método NBI também é relatado em Duarte Costa *et al*. (2016) e em Lopes *et al*. (2016).

A análise de correlação é fundamental para a construção da fronteira de Pareto por meio de algoritmos de otimização. Uma vez que a fronteira é obtida por meio da ponderação entre funções com dois ou mais objetivos, os pesos serão igualmente divididos para atendê-los simultaneamente, entretanto, se existir correlação e se ela for negligenciada, respostas ótimas serão obtidas, mas não condizentes com a realidade. Desse modo, é possível obter uma fronteira de Pareto composta por soluções viáveis, porém irreais.

Diante deste fato e com embasamento em Duarte Costa *et al*. (2016) e em Lopes *et al*. (2016), a utilização da Análise de Componentes Principais (ACP), do inglês *Principal Component Analysis*, que se refere a uma técnica estatística multivariada de redução de dimensionalidade sem perda da informação contida no conjunto original de variáveis, proporciona o tratamento da dependência entre múltiplas funções objetivas e neutraliza os efeitos sobre os coeficientes de correlação. (PAIVA *et al*. (2012)).

Desse modo, este trabalho foca no uso da análise de componentes principais com o propósito de eliminar a correlação entre as respostas modeladas pelos estimadores robustos. Este novo conjunto de dados, chamado escores de componentes principais, são úteis para construção de novas superfícies de resposta não correlacionadas. Esta abordagem almeja eliminar problemas na construção da fronteira de Pareto conforme ilustrado na próxima seção.

1.2.1 Objeto de estudo

As fronteiras de Pareto ilustradas a seguir são provenientes da otimização do processo de

torneamento do aço de corte fácil ABNT/SAE 12L14 em que a resposta avaliada foi a rugosidade superficial (R_a). A otimização realizada é proveniente das respostas modeladas pelos pares de estimadores mencionados na Tabela 1. Desse modo, a partir das respostas informadas na Tabela 2, otimizações foram realizadas pelo método NBI, pela restrição normal normalizada, do inglês *Normalized Normal Constraint* (NNC), e pelo comprimento da homotopia de arco, do inglês *Arc Homotopy Length* (AHL). Esses métodos de otimização forma selecionados uma vez que são apontados por proporcionarem um conjunto de soluções uniformemente espaçadas na fronteira de Pareto e, assim, obtendo um melhor desempenho em problemas multiobjetivos. (MESSAC *et al*., 2003; PEREIRA *et al*., 2013)

Tabela 2 – Valores obtidos de R_a pela modelagem dos estimadores

$\bar{x}$	s	$\tilde{x}$	MAD	$\tilde{x}_{H2}$	S_{H2}	HL_n	S_n	Q_n	$\tilde{x}_\tau$	s_τ	$\tilde{x}_{MLE}$	s_{MLE}
1.356	0.923	0.927	0.241	1.192	0.600	1.163	0.282	0.342	0.865	0.306	1.681	0.708
1.648	1.049	1.193	0.668	1.562	0.983	1.496	0.730	0.849	1.189	0.781	1.903	0.890
1.782	0.664	1.740	0.549	1.695	0.514	1.710	0.514	0.550	1.643	0.507	1.881	0.597
1.839	0.643	1.703	0.534	1.792	0.611	1.783	0.682	0.591	1.670	0.559	1.904	0.574
2.220	2.377	1.460	0.266	1.602	0.447	1.534	0.254	0.322	1.417	0.315	3.234	1.593
2.199	1.833	1.455	0.469	1.832	1.086	1.558	0.514	0.614	1.347	0.557	2.620	1.338
1.817	0.431	1.681	0.173	1.728	0.201	1.728	0.158	0.174	1.678	0.184	1.941	0.305
2.235	1.223	1.643	0.115	1.892	0.534	1.704	0.110	0.134	1.628	0.140	2.624	0.822
1.897	1.131	1.465	0.316	1.558	0.411	1.528	0.405	0.402	1.435	0.349	2.290	0.897
2.079	1.406	1.630	0.680	1.759	0.812	1.697	0.777	0.809	1.526	0.728	2.446	1.212
1.846	0.925	1.670	0.607	1.745	0.781	1.707	0.875	1.004	1.616	0.687	1.880	0.844
1.847	0.566	1.721	0.340	1.754	0.370	1.731	0.325	0.351	1.682	0.347	1.945	0.441
1.680	0.586	1.470	0.502	1.680	0.664	1.717	0.674	0.437	1.496	0.600	1.725	0.501
2.301	1.142	2.276	1.245	2.160	0.910	2.047	1.266	1.038	2.098	1.016	2.454	0.904
2.319	1.521	2.118	1.115	2.040	0.870	0.542	1.098	1.077	1.934	0.936	2.852	1.251
2.233	1.433	2.075	1.129	1.986	0.884	2.007	1.148	1.070	1.882	0.949	2.533	1.061
2.257	1.442	2.236	1.505	2.058	1.076	2.071	1.453	1.115	1.979	1.216	2.443	1.158

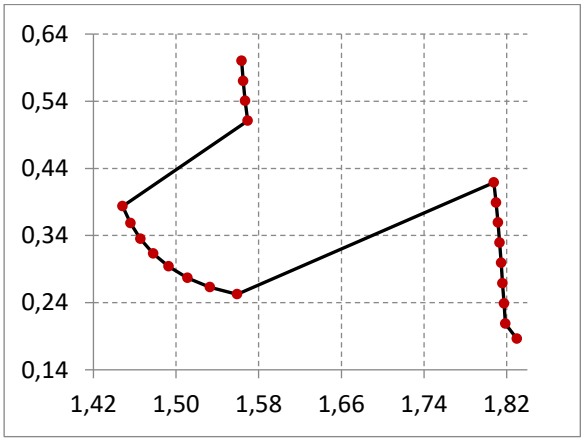

Figura 1 – Fronteira de Pareto (NBI): $\bar{x}$ x S

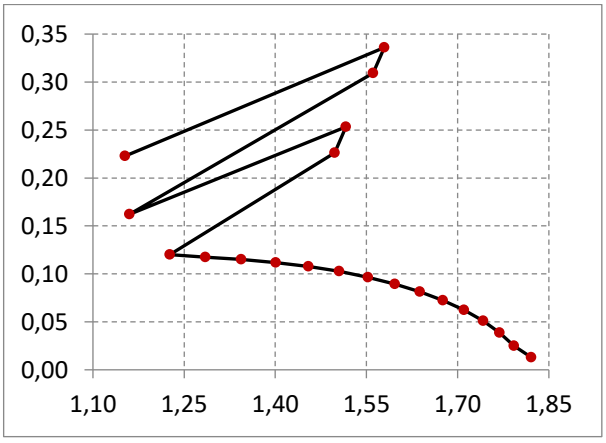

Figura 2 – Fronteira de Pareto (NBI): $\tilde{x}$ x MAD

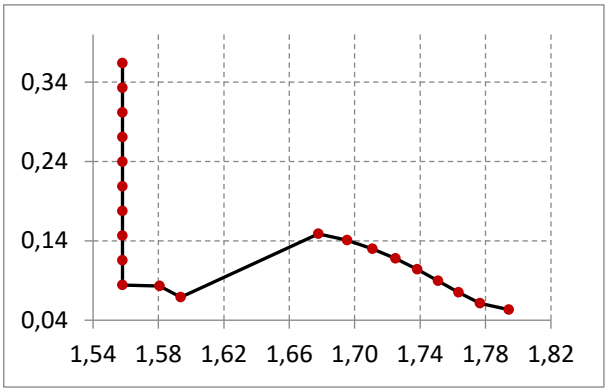

Figura 3 – Fronteira de Pareto (NBI): $\tilde{x}_{H2}$ x s_{H2}

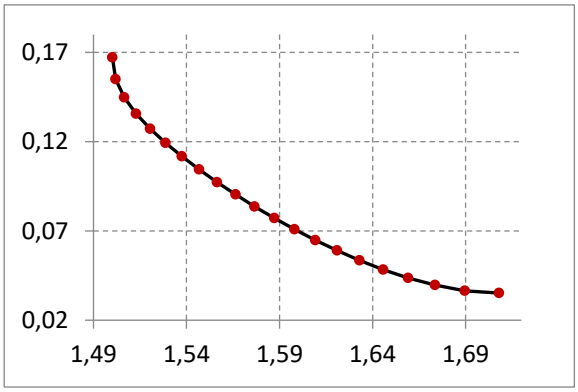

Figura 4 – Fronteira de Pareto (NBI): HL_n x s_n

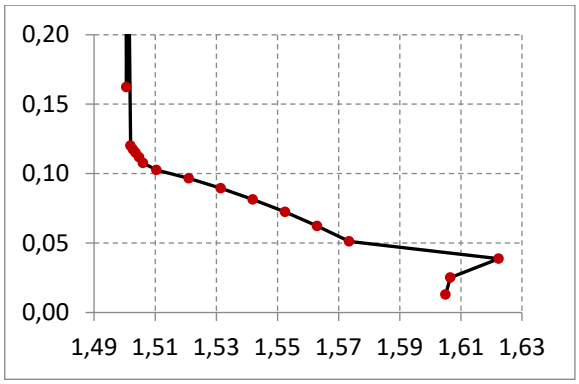

Figura 5 – Fronteira de Pareto (NBI): HL_n x Q_n

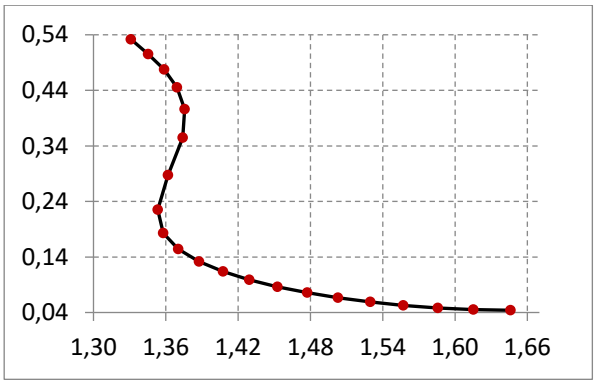

Figura 6 – Fronteira de Pareto (NBI): $\tilde{x}_{\tau}$ x s_{τ}

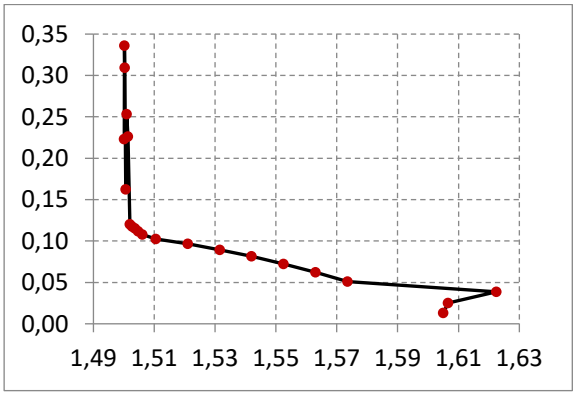

Figura 7 – Fronteira de Pareto (NBI): HL_n x MAD

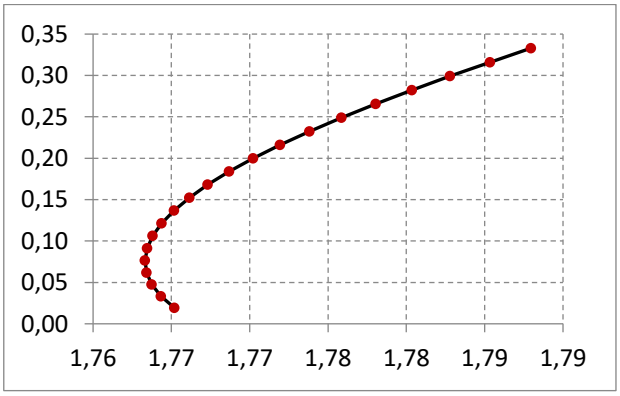

Figura 8 – Fronteira de Pareto (NBI): $\tilde{x}_{MLE}$ x s_{MLE}

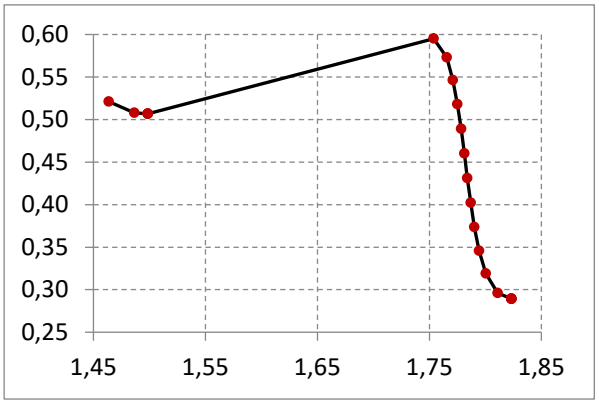

Figura 9 – Fronteira de Pareto (NNC): $\bar{x}$ x s

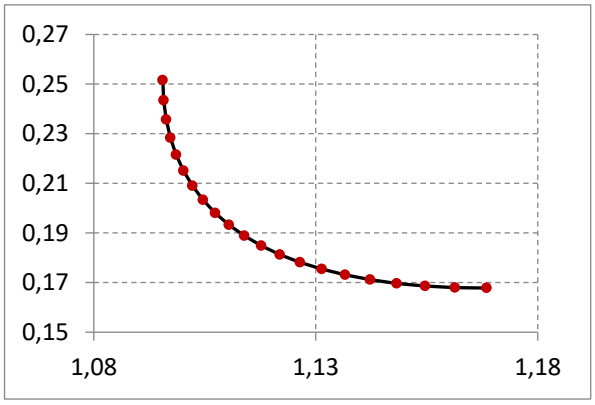

Figura 10 – Fronteira de Pareto (NNC): $\tilde{x}$ x MAD

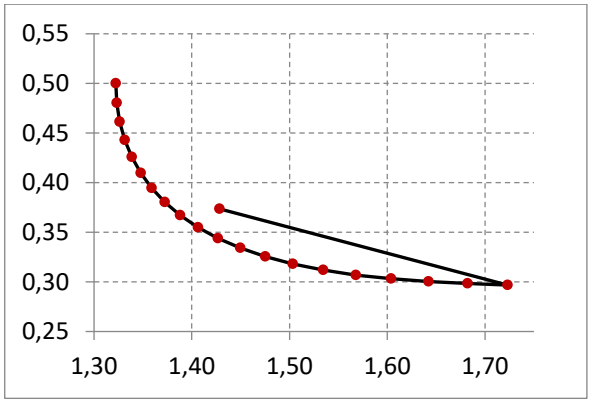

Figura 11 – Fronteira de Pareto (NNC): $\tilde{x}_{H2}$ x s_{H2}

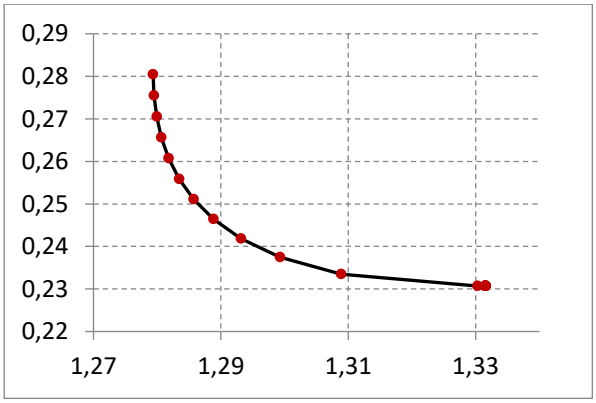

Figura 12 – Fronteira de Pareto (NNC): HL_n x s_n

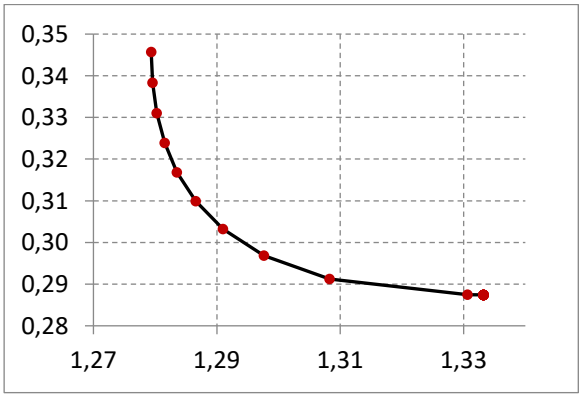

Figura 13 – Fronteira de Pareto (NNC): HL_n x Q_n

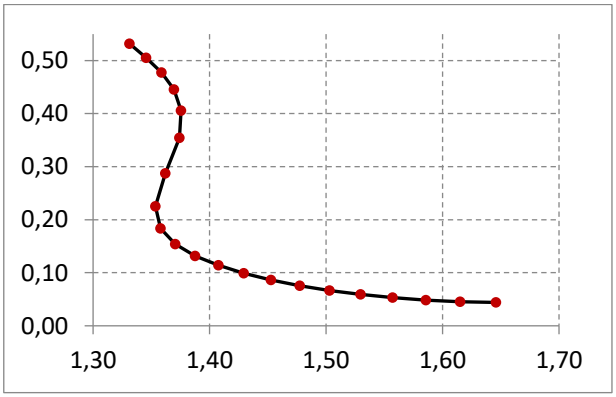

Figura 14 – Fronteira de Pareto (NNC): $\tilde{x}_\tau$ x s_τ

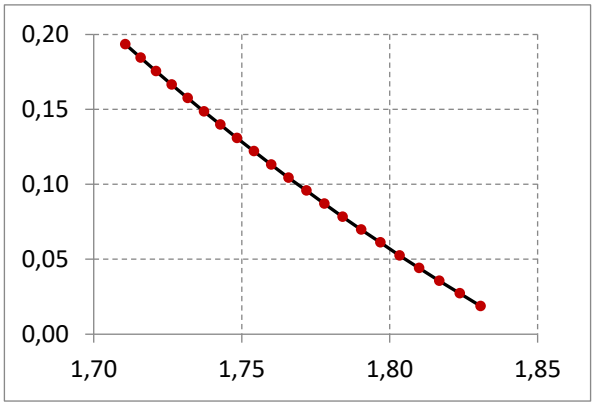

Figura 15 – Fronteira de Pareto (NNC): HL_n x MAD

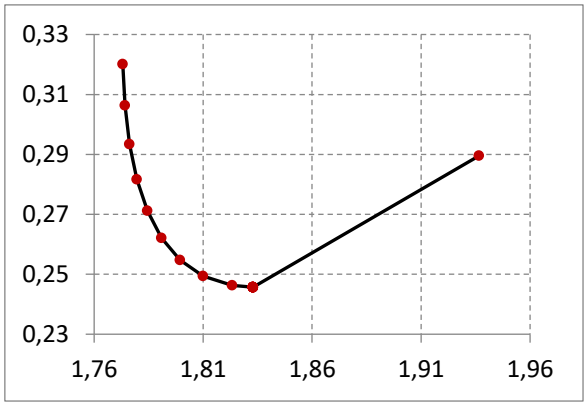

Figura 16 – Fronteira de Pareto (NNC): $\tilde{x}_{MLE}$ x s_{MLE}

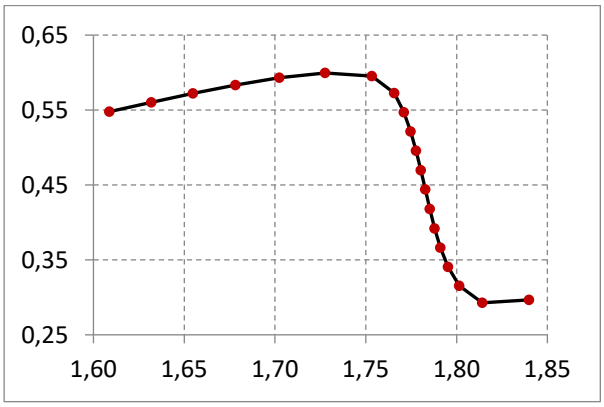

Figura 17 – Fronteira de Pareto (AHL): $\bar{x}$ x s

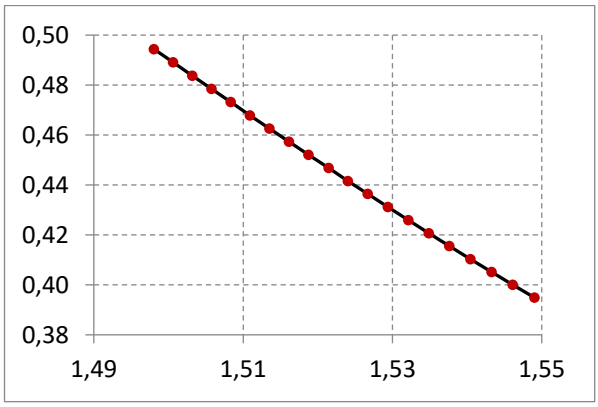

Figura 18 – Fronteira de Pareto (AHL): $\tilde{x}$ x MAD

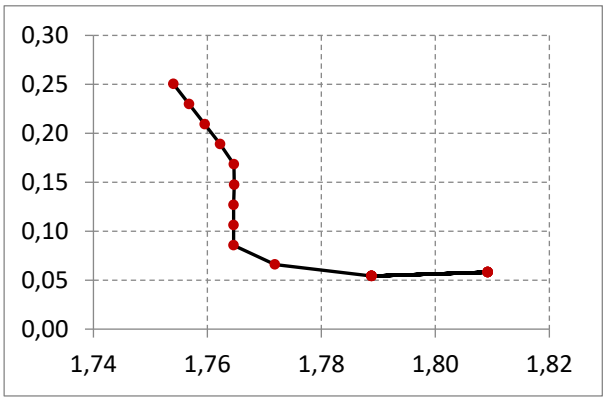

Figura 19 – Fronteira de Pareto (AHL): $\tilde{x}_{H2}$ x s_{H2}

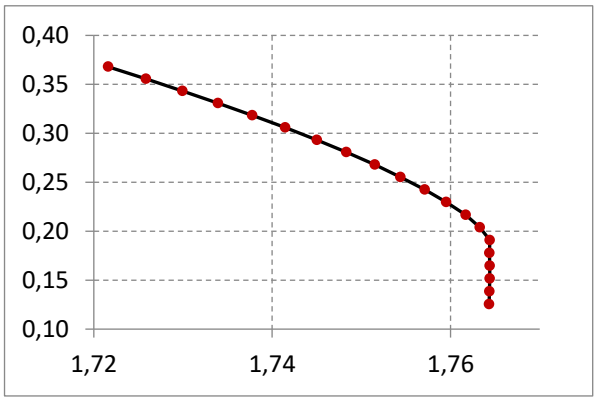

Figura 20 – Fronteira de Pareto (AHL): HL_n x s_n

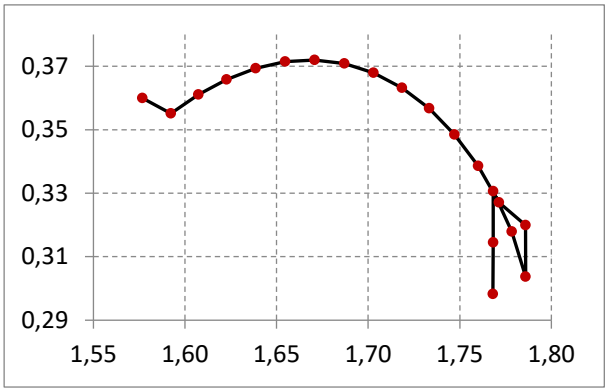

Figura 21 – Fronteira de Pareto (AHL): HL_n x Q_n

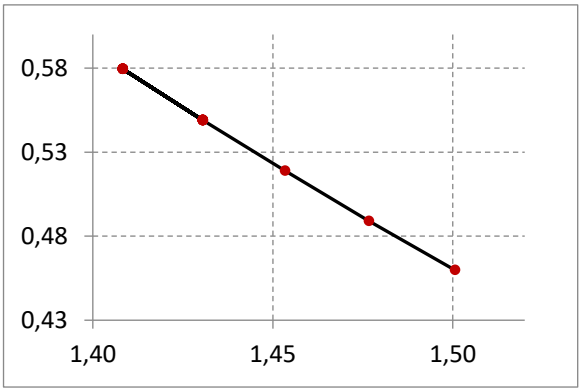

Figura 22 – Fronteira de Pareto (AHL): $\tilde{x}_\tau$ x s_τ

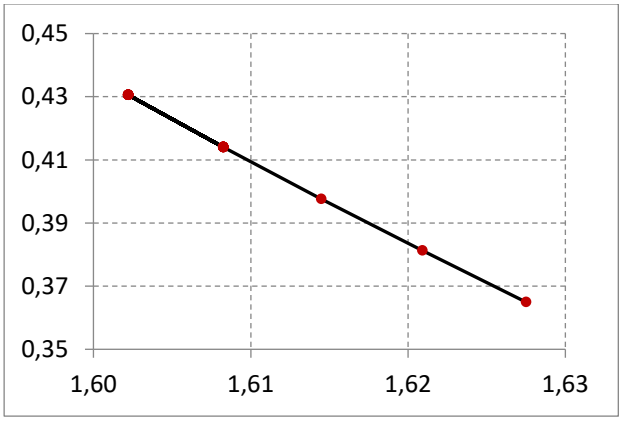

Figura 23 – Fronteira de Pareto (AHL): HL_n x MAD

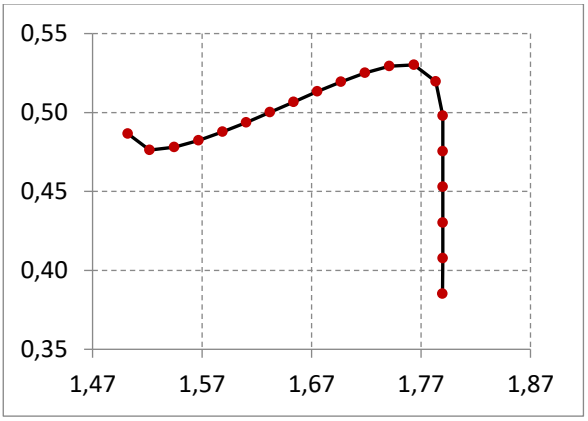

Figura 24 – Fronteira de Pareto (AHL): $\tilde{x}_{MLE}$ x s_{MLE}

Desse modo, é possível notar que nem todos os pares de estimadores proporcionaram fronteiras de Pareto convexas e equiespaçadas independente do método de otimização utilizado. Portanto, este presente trabalho demonstra a contribuição de se utilizar a técnica de componentes principais juntamente com a modelagem de funções duais por meio do Erro Quadrático Médio Multivariado (EQMM) com o intuito de obter funções objetivo não correlacionadas em termos de escores. Este fato implica em soluções ótimas que satisfaçam todas as restrições e, assim, proporcionando valores ideais das variáveis de entrada do processo analisado.

A preocupação com a etapa de modelagem será o foco desta tese uma vez que todos os procedimentos que precedem a fase de otimização devem ser executados corretamente com o objetivo de encontrar a solução ótima que satisfaça todas as restrições impostas.

1.3 Objetivos

De acordo com a contextualização apresentada, este trabalho foi desenvolvido com o propósito de atingir os objetivos apresentados nesta seção.

1.3.1 Objetivo geral

Validação de um algoritmo de otimização multiobjetivo baseado no agrupamento de respostas correlacionadas e modeladas por estimadores robustos.

1.3.2 Objetivos específicos

Com o intuito de cumprir com o objetivo geral deste trabalho, os seguintes objetivos específicos devem ser alcançados:

- Obter fronteiras convexas e equiespaçadas de Pareto por meio de técnicas estatísticas multivariadas combinadas com o método NBI;
- Verificar se a otimização realizada por componentes principais que consideram a melhor explicação dos estimadores robustos, possui um melhor conjunto de respostas Pareto-ótimas em relação à otimização realizada em Gaudêncio (2015) que priorizou a comparação entre eles;
- Comparar o método de otimização proposto com demais técnicas conhecidas de otimização a fim de validar a robustez do algoritmo;
- Substituir funções de teste no lugar das respostas do processo de manufatura objeto de estudo a fim de validar o método proposto em outros cenários.

1.4 Limitações do trabalho

Neste trabalho, propõe-se que a comparação entre os algoritmos de otimização será realizada exclusivamente pelas fronteiras de Pareto que representarão os pontos ótimos do problema. Ainda, o único algoritmo aplicado na otimização das respostas será o método do Gradiente Reduzido Generalizado (GRG) e, para isso, somente serão utilizados modelos de 2ª ordem. A otimização realizada pelo algoritmo genético foi apenas para fins de comparação.

Conforme apresentado, o objeto de estudo deste trabalho limitou-se ao processo de torneamento do aço de corte fácil ABNT/SAE 12L14 o qual foi baseado em um arranjo cruzado e a resposta – rugosidade - deste processo será modelada, exclusivamente, pelos estimadores descritos na Tabela 1.

Por sua vez, estas respostas modeladas serão agrupadas de acordo com a estrutura de correlação existente entre elas pela análise de *cluster* por meio do método *Ward Linkage*; único critério hierárquico de aglomeração adotado.

Após o agrupamento das respostas, o método de otimização escolhido para gerar as fronteiras de Pareto será a Interseção Normal à Fronteira – NBI com o auxílio de funções obtidas pelo Erro Quadrático Médio Multivariado (EQMM) o qual combina as técnicas da metodologia de superfície de resposta e componentes principais.

2. ARTIGOS PUBLICADOS E SUBMETIDOS

Os artigos apresentados nesta seção exemplificam a proposta e, bem como, os objetivos desta tese. Desse modo, o primeiro artigo intitulado "*A multiobjective optimization model for machining quality in the AISI 12L14 steel turning process using fuzzy multivariate mean square error*" foi aceito e publicado no periódico *Precision Engineering* (Elsevier) o qual possui classificação A2 no quadriênio 2013-2016 Qualis/CAPES.

O segundo artigo intitulado "*Fuzzy multivariate mean square error in equispaced Pareto frontiers considering manufacturing process optimization problems*" foi aceito e publicado no periódico *Engineering with Computers* (Springer) o qual possui classificação B1 no quadriênio 2013-2016 Qualis/CAPES.

Por fim, o terceiro artigo intitulado "*Method for multiobjective optimization with Pareto boundaries using fuzzy decision maker*" foi submetido ao periódico *Applied Soft Computing* (Elsevier) o qual possui classificação A2 no quadriênio 2013-2016 Qualis/CAPES.

2.1 Artigo publicado na *Precision Engineering*

A contribuição deste artigo está na proposta de um método de otimização multiobjetivo que utiliza a análise de componentes principais para minimizar a redundância de funções objetivas em termos do erro quadrático médio multivariado, possibilitando uma melhor explicação do valor alvo e da dispersão da resposta em termos dos estimadores propostos.

Em um nível de confiança de 95%, o valor otimizado se enquadra dentro dos intervalos de confiança multivariados apenas para o Modelo B, no qual a modelagem realizada pela mediana e pelo MAD (*Median Absolute Deviation*) é considerada e assim, afirmando qual par de estimadores atinge a solução mais robusta. Através da pesquisa proposta, o modelo desenvolvido pode ser utilizado em indústrias para determinação de parâmetros de usinagem com alta qualidade, acarretando em baixas rugosidades.

Comparativos foram realizados com o propósito de validar a resposta ótima obtida para o processo de torneamento ABNT/SAE 12L14. Primeiramente, a rugosidade superficial do corpo de prova obtida pelos parâmetros ótimos de usinagem foi comparada com a rugosidade de um corpo de prova usinado com outros valores de parâmetros de entrada e assim, validando a resposta obtida pelo algoritmo de otimização proposto. Em sequência, foi realizada uma otimização multiobjetivo pelo algoritmo genético (função *gamultiobj*) com o propósito de se comparar os resultados e reafirmar a eficiência do algoritmo proposto.

A multiobjective optimization model for machining quality in the AISI 12L14 steel turning process using fuzzy multivariate mean square error

Juliana Helena Daroz Gaudêncio[a*], Fabrício Alves de Almeida[a], João Batista Turrioni[a], Roberto da Costa Quinino[b], Pedro Paulo Balestrassi[a], Anderson Paulo de Paiva[a]

[a] Institute of Industrial Engineering and Management, Federal University of Itajubá, Itajubá-MG, 37500-903, Brazil

[b] Department of Statistics, Federal University of Minas Gerais, Belo Horizonte-MG, 31270-901, Brazil

[*] Corresponding author: juliana_hdg@yahoo.com.br; +55 35 99139-1577

https://doi.org/10.1016/j.precisioneng.2019.01.001

Abstract

Organizations focus on determining optimal operating conditions to ensure quality; however, industrial processes exhibit a high degree of variability and the use of robust estimators is a suitable alternative to model experimental data. As a case study, the surface roughness (R_a) of an AISI 12L14 steel turning process is optimized to find a centrality measure close to its target with minimum dispersion and thus improve the quality of the machined surface by choosing the best values of the associated parameters. The main contribution of this research is the proposal of a multiobjective optimization method that uses principal components analysis to minimize the redundancy of objective functions in terms of multivariate mean square error, thus making optimization of the process possible with a better explanation of all centrality and dispersion estimators proposed herein. The method uses a fuzzy decision maker to show the surface roughness' optimum result with the most efficient production taken into consideration. To prove its efficiency, confirmation runs were conducted. At a confidence level of 95%, the optimal value falls within the multivariate confidence intervals only for Model B, in which the estimators' median and median absolute deviation are considered, thus affirming which pair of estimators achieves the most robust parameter design solution. Through the proposed research, the developed model can be used in industries for determining machining parameters to attain high quality with minimum power consumption and hence maximum productivity.

Keywords

Robust Parameter Design; Normal Boundary Intersection; Principal Components Analysis; Fuzzy Decision Maker.

2.2 Artigo publicado na *Engineering with Computers*

Diferentemente do artigo submetido à *Precision Engineering*, a modelagem neste segundo artigo foi realizada nas respostas originais do processo de usinagem objeto de estudo. Respostas tais como o custo total, vida útil da ferramenta, tempo total de usinagem, temperatura de corte, energia de corte e ruído foram consideradas.

Este artigo foca na abordagem combinada do método de otimização NBI com o erro quadrático médio multivariado (MMSE), tornando-se uma abordagem que supera o tradicional NBI na construção de fronteiras de Pareto convexas e equiespaçadas e, também, obtendo uma redução considerável no número de iterações de respostas a serem otimizadas.

Para fins de comparação, o desempenho dos métodos de otimização comprimento da homotopia de arco, critério global e somas ponderadas foram explorados. Para ilustrar esta proposta, o processo de torneamento de aço temperado AISI H13 é utilizado considerando a ferramenta CC670. Resultados experimentais indicam que a solução encontrada pela abordagem NBI-MMSE é mais apropriada e supera todos os métodos concorrentes de otimização. Além disso, este algoritmo também foi testado em funções de teste para confirmar a sua eficiência.

Fuzzy Multivariate Mean Square Error in Equispaced Pareto Frontiers Considering Manufacturing Process Optimization Problems

Juliana Helena Daroz Gaudêncio[1], Fabrício Alves de Almeida[1*], Rachel Campos Sabioni[2], João Batista Turrioni[1], Anderson Paulo de Paiva[1], Paulo Henrique da Silva Campos[1]

[1]Institute of Industrial Engineering and Management, Federal University of Itajubá, Itajubá, Brazil;
[2]Department of Mechanical Engineering, Sorbonne University, University of Technology of Compiègne, France.
* Corresponding author: fabricio.alvesdealmeida@gmail.com

https://doi.org/10.1007/s00366-018-0660-0

Abstract: This paper proposes a combined approach using the normal boundary intersection (NBI) and multivariate mean square error (MMSE) that is an alternative approach to outperform the traditional NBI driving to an equispaced Pareto Frontier in a low-dimension space with a considerable reduction in the number of iterations. The method participating in the evolutionary stage of creating a uniformly spread Pareto Frontier for a nonlinear multiobjective problem is the NBI using normalized objective functions allied to MMSE. In sequence, the fuzzy MMSE approach is utilized to determine the optimal point of the multi-objective optimization. For sake of comparison, the performance of arc homotopy length, global criterion method, and weighted sums were explored. To illustrate this proposal, a multivariate case of AISI H13 hardened steel turning process is used. Experimental results indicate that the solution found by NBI-MMSE approach is a more appropriate Pareto frontier that surpassed all the competitors and also provides the best compromised solution to set the machine input parameters. Further, this algorithm was also tested in benchmark functions to confirm the NBI-MMSE efficiency.

Keywords: Principal component analysis; Multivariate mean square error; Normal boundary intersection; Fuzzy decision maker; Hardened steel turning.

2.3 Artigo submetido na *Applied Soft Computing*

Considerando o mesmo processo de torneamento de aço temperado AISI H13 do artigo publicado na *Engineering with Computers*, mas realizado com uma ferramenta diferente, a PCBN 7025; este artigo possui o objetivo de reforçar a robustez do algoritmo de otimização proposto NBI-MMSE em que a dimensionalidade do problema é reduzida e a correlação entre as múltiplas respostas é eliminada. Seis variáveis de saída foram consideradas: vida útil da ferramenta, custo total, rugosidade superficial, força, ruído e energia de corte.

O algoritmo de otimização proposto foi comparado com os métodos da restrição normal normalizada, comprimento da homotopia de arco, critério global e *desirability*. Os resultados mostram que o NBI-MMSE tem um desempenho superior e, bem como, demais funções de teste foram utilizadas para avaliar a eficácia e robustez do algoritmo. Portanto, o NBI-MMSE identifica a dinâmica do processo de torneamento do aço AISI H13 revelando soluções ideais para os parâmetros do processo de entrada.

Method for multiobjective optimization with Pareto boundaries using fuzzy decision maker

Juliana Helena Daroz Gaudêncio[a*], João Éderson Corrêa[a], Vinícius de Carvalho Paes[a], João Batista Turrioni[a], Anderson Paulo de Paiva[a], Paulo Henrique da Silva Campos[a]

[a] Institute of Industrial Engineering and Management, Federal University of Itajubá, Itajubá-MG, 37500-903, Brazil

[*] Corresponding author: juliana_hdg@yahoo.com.br; +55 35 99139-1577

Abstract

This work presents the process of AISI H13 hardened steel turning with the PCBN 7025 tool, considering six output variables: tool life, machining total cost, surface roughness, machining force, sound pressure level, and specific cutting energy. Several problems are encountered in engineering processes that have adverse effects on the reliability of complex engineering systems. Hence, the aim of this work is to optimize the hardened steel turning process by applying mathematical methods to reduce dimensionality and eliminate the correlation between the multiple responses. The resultant latent response surfaces and their respective targets constitute the normalized multivariate mean square error (MMSE) function that is minimized by the normal boundary intersection (NBI) method. Furthermore, a fuzzy algorithm is applied to identify the best solution from several feasible solutions of the Pareto frontier that is compared with the performances of normalized normal constraint, arc homotopy length, global criterion method, and desirability method. The results show that NBI-MMSE has a higher performance than the other methods. In addition, NBI-MMSE is tested with benchmark functions to evaluate its effectiveness and robustness. Therefore, NBI-MMSE identifies the dynamics of the turning process of AISI H13 steel by revealing the optimal solutions for the input process parameters.

Keywords

Principal Component Analysis; Normal Boundary Intersection; Multivariate Mean Square Error; Fuzzy Decision Maker.

1. Introduction

Manufacturing processes have undergone considerable changes to accommodate various client's expectations. They require constant attention and a great deal of effort from suppliers to meet the burgeoning demands. However, these challenges involving quality of goods, process variability, cost reduction, short cycle times, large production rates, manufacturability, sustainability and competitiveness (Lin *et al*. 2015; Su *et al*. 2015) can only be addressed using trade-off strategies, and a tightly-controlled and continuous improvement.

An effective way of solving this challenge involves the study of process parameters, product characteristics, and latent relationships. The perspectives can then be clarified and the decision-making process improved mathematically by combining a series of experimental strategies, statistical analyses, and optimization techniques. In this case, Design of Experiments (DOE) provides a collection of experimental techniques capable of statistically evaluating the influence of process parameters and establishing a functional relationship between the process factors and responses, using a minimum number of experiments (He *et al*. 2009; Montgomery 2012). There are several techniques for the modeling and analysis of a second-order response surface. The most widely used is the rotatable central composite design (CCD) which explores the spherical region of a response around the levels of its input parameters to produce nonlinear equations. These equations act as objective functions for continuous variables in any optimization algorithm to find the optimal operating conditions and produce better results (Ansoni and Seleghim Jr., 2016, Lopez *et al*., 2014; Zidani *et al*., 2013). Thus, many real-life engineering design problems can be formulated as multiobjective optimization or Pareto optimization (Kelesoglu, 2007).

The normal boundary intersection (NBI) method (Das and Dennis, 1998) and response surface methodology (RSM) have been used extensively in the multiobjective optimization of many manufacturing processes such as dry end milling (Costa *et al*., 2016a; Lopes *et al*., 2016), aluminum alloys helical milling (Pereira *et al*., 2017b), hardened steel turning (Rocha *et al*., 2017; Paiva *et al*., 2014), free-machining steel turning (Costa *et al*., 2016b), cast iron vertical turning (Rocha *et al*., 2015), and pulsed gas metal arc welding (P-GMAW) (Carvalho *et al*., 2016). Several researches have revealed the correlations among several responses. Box *et al*. (1973) discussed the impact of the correlation of multiresponse data on the accuracy of the regression models and the optimization results. Typically, when correlated output variables are the independent variables during coefficients estimation, a bias (Lopes *et al*., 2016) is

introduced to each element of the coefficients vector $\hat{\boldsymbol{\beta}}$, which promotes a deviation from the real optimum during the iterations, thereby resulting in an inversion of the correlation..

To avoid these effects, Paiva *et al*. (2012) suggested the replacement of the original *p* columns of $\mathbf{Y}_{(nxp)}$ matrix in the ordinary least squares (OLS) algorithm by (*p*-*r*) latent variables ξ_{score}^{i} obtained from variance-covariance (**Σ**) or correlation (**R**) matrices of the multiresponse data, where *p* is the number of responses and *r* is number of suppressed dimensions. This procedure is known as principal component analysis (PCA). For strong correlations, the number of significant principal components (*p*-*r*) is generally less than two due to the redundancy of **Σ** or **R** (with $p < r$). The replacement produces a vector of coefficients $\tilde{\boldsymbol{\beta}} \neq \hat{\boldsymbol{\beta}}$. Therefore, the original *p* objective functions become principal component score (ξ_{score}^{i}) functions whose optimization produce better results. Several works have shown the utility and accuracy of PCA as a low-dimensional optimization strategy (Rocha *et al*., 2017; Brito *et al*., 2017; Costa *et al*., 2016a; Pereira *et al*., 2017b; Paiva *et al*., 2014).

However, Paiva *et al*. (2012) proposed the Multivariate Mean Square Error function [$MMSE_i(\mathbf{x})$] as a means of using PCA to solve target-based problems. $MMSE_i(\mathbf{x})$ is an index which combines the most significant latent response surfaces and its respective targets using a squared difference. When more than one principal component (PC) is required to perform 80% of the variance-covariance transformations, a geometric mean may be used to aggregate the latent variables.

Therefore, this study presents the NBI-MMSE method for the multiobjective optimization of correlated multiresponse data. In this case, normalized $MMSE_i(\mathbf{x})$ functions are minimized by NBI while successive solutions are obtained at different degrees of importance (w_i), resulting in a series of feasible solutions graphically summarized by an equidistant multivariate Pareto frontier. The aim is to demonstrate the advantages of the method over traditional methods by using few iterations in a low-dimensional space.

Furthermore, AISI H13 hardened steel turning process was done using PCBN 7025 hexagonal tools, to estimate the accuracy of the method and explore other areas of application. The process was investigated using a CCD for three process variables such as cutting speed (V_c), cutting feed (*f*), and machining depth (A_p), in a rotatable set of 19 experiments. The study considered six responses organized in four dimensions: quality (surface roughness (R_a)) (Buczkowski and Kleiber, 2009), productivity (specific cutting energy (SCE) and cutting force (F_r)), economic feasibility (process costs (K_p) and tool life (T)), and labor health (sound pressure level (SPL)). Most responses had significant correlations, thereby supporting the use of PCA.

Moreover, four alternative methods such as normalized normal constraint (NNC) method, arc homotopy length (AHL) method, global criterion method (GCM), and desirability method were compared to explore the performance of NBI-MMSE. In this case, NNC and AHL utilized normalized $MMSE_i(\mathbf{x})$ functions, while GCM and desirability utilized the functions of the original response surfaces. Confirmation tests and hypothesis tests were then carried out on NBI-MMSE . Finally, a series of tests were performed to judge the performance of NBI-MMSE using generic benchmark objective functions (nonlinear, continuous, differentiable, separable, scalable, unimodal and correlated). In the following sections, we will describe the details of this multivariate framework.

2. NBI-MMSE method

The steps outlined below demonstrate how NBI-MMSE method can be used to find feasible solutions for correlated multiresponse data.

***Step 1*:** Design and execute a suitable experimental design based on the most prominent factors of the process and the responses. Store the results.

***Step 2*:** Find the correlations among several responses to verify if the variance-covariance matrix supports PCA.

***Step 3*:** Perform PCA by obtaining the PC_{score} from the original responses and store the respective eigenvalues λ_{PC} and eigenvectors e_{ij}. Determine the quadratic models of the latent variables (ξ_{score}^{i}) using OLS algorithm.

***Step 4*:** Perform individual optimization of the original responses and construct the *payoff* matrix. Define the targets for the original responses.

***Step 5*:** Execute the individual optimization function $PC_{score}^{i}(\mathbf{x})$ to determine the $MMSE_T(\mathbf{x})$. Construct its *payoff* matrix.

***Step 6*:** Normalize $MMSE_i(x)$ using the Utopia $\left(MMSE_i^U(\mathbf{x})\right)$ and Pseudo-Nadir ($MMSE_i^N(\mathbf{x})$) points according to Eq. (1).

$$\bar{f}i(x) = \frac{f_i(x) - f_i^U}{f_i^N - f_i^U} \Rightarrow \begin{cases} \bar{f}_1(x) = \overline{MMSE}_1(x) = \dfrac{MMSE_1(x) - MMSE_1^U}{MMSE_1^N - MMSE_1^U} \\ \bar{f}_2(x) = \overline{MMSE}_2(x) = \dfrac{MMSE_2(x) - MMSE_2^U}{MMSE_2^N - MMSE_2^U} \end{cases} \quad (1)$$

***Step 7*:** Run the optimization of the NBI-MMSE system described by Eq. (21). Repeat this procedure for different weights to generate all feasible points of the Pareto frontier. Here,

we have used the generalized reduced gradient (GRG) for the optimization of a "solution space" constraint.

Step 8: Define the optimal Pareto solution. After executing all iterations of the algorithm, choose the best solution using the highest value of the total fuzzy membership function of $MMSE_T(\mathbf{x})$.

Step 9: Execute confirmation tests to verify the compatibility of the theoretical and experimental data optimization results.

Fig. 1 illustrates the nine steps of the NBI-MMSE approach.

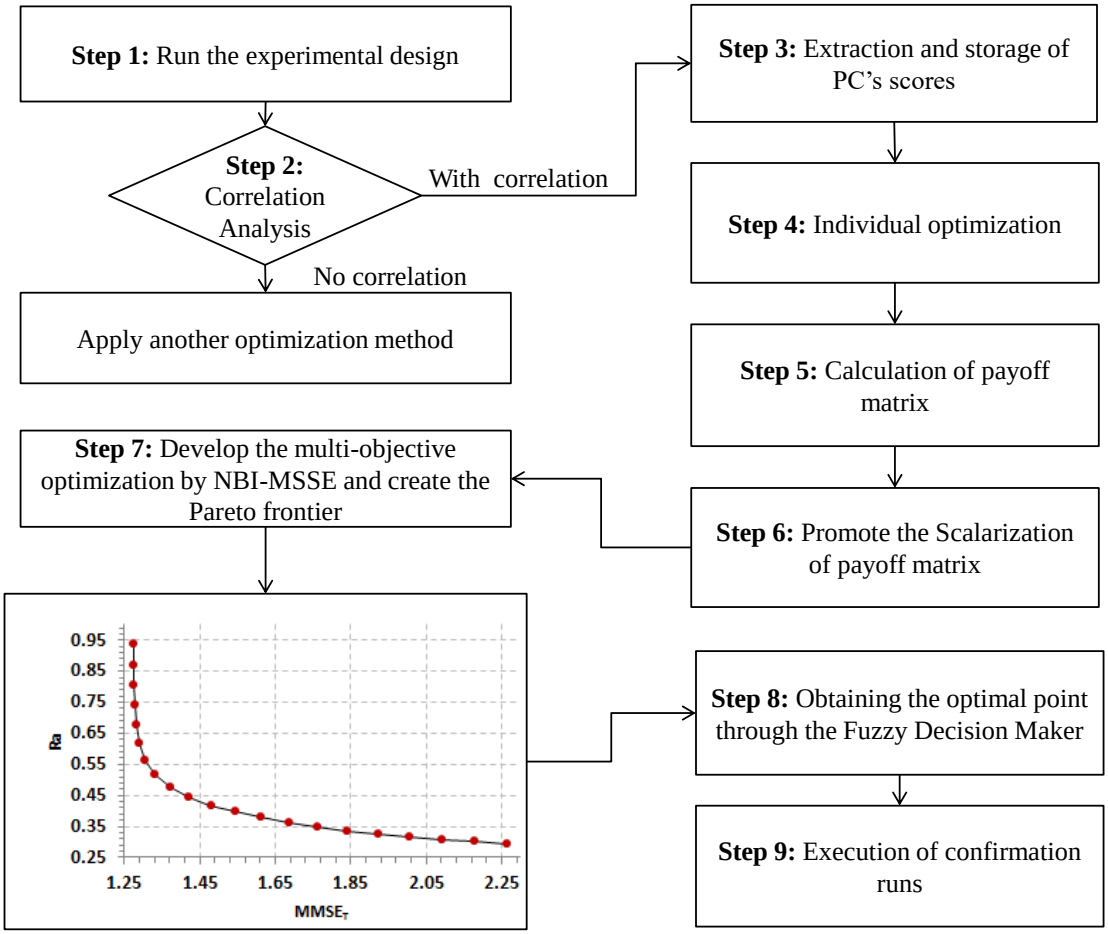

Figure 1: Overview of the proposed procedure

3. Statistical and optimization background

This section introduces the statistical and optimization techniques for the NBI-MMSE method. We also describe the relationships among these techniques and how multivariate approaches may replace traditional multiobjective optimization frameworks.

3.1. The Principal Component Analysis (PCA)

PCA is a multivariate statistical technique which reduces the dimensionality of a dataset while preserving the information of the original variables (Rapcsák, 2004; Haridy *et al.*, 2011; Xian *et al*., 2013; Paiva *et al.*, 2014). PCA has been used extensively to reduce the dependence between multiple objective functions and neutralize the correlation effects of the coefficients of objective functions (Paiva *et al.*, 2012).

Suppose $f_1(\boldsymbol{x}), f_2(\boldsymbol{x}), f_3(\boldsymbol{x})$ are correlated functions written in terms of random DOE response vector $\mathbf{Y^T} = \left[\mathbf{Y_1}, \mathbf{Y_2}, \ldots, \mathbf{Y_p}\right]$. $\boldsymbol{\Sigma}$ is the variance-covariance matrix associated with this vector which can be factorized into pairs of eigenvalues–eigenvectors $(\lambda_i, e_i), \ldots \geq (\lambda_p, e_p)$, with eigenvalues $\lambda_1 \geq \lambda_2 \geq \cdots \geq \lambda_p \geq 0$. The i[th] PC will be the linear combination $\left(\mathbf{PC}_i = \ell_i^{\mathbf{T}}\mathbf{x}\right)$ that maximizes the variance $Var\left(\ell_i^{\mathbf{T}}\mathbf{x}\right)$. The PC is then written as:

$$\begin{aligned} &\underset{\mathrm{x}\in\Omega}{Max} \quad f(\mathbf{x}) = Var\left(\ell_i^{\mathbf{T}}\mathbf{x}\right) = \ell_i^{\mathbf{T}}\left(\boldsymbol{\Sigma}_{\mathbf{x}}\right)\ell_i \\ &S.t.: \quad g_1(\mathbf{x}) = \ell_i^{\mathbf{T}}\,\ell_i = 1 \\ &\qquad\quad g_2(\mathbf{x}) = Cov(\ell_i^{\mathbf{T}}\mathbf{x}, \ell_j^{\mathbf{T}}\mathbf{x}) = 0 \\ &With: Cov(\ell_i^{\mathbf{T}}\mathbf{x}, \ell_j^{\mathbf{T}}\mathbf{x}) = \ell_j{}^{\mathbf{T}}\left[\boldsymbol{\Sigma}_{\mathbf{x}}\right]\ell_j = \sum_{i=1}^{J}\sum_{j=1}^{J}\ell_i\ell_j\sigma_{ij} \end{aligned} \tag{2}$$

Eq. (2) emphasizes the development of PCs by solving a nonlinear constrained optimization problem. In this case, the *i[th]* Lagrange multiplier coincides with the *i[th]* eigenvalue of variance-covariance matrix, yielding an optimum value, **x***. PCA can also be applied on a correlation matrix [**R**] where the off-diagonal elements of [**R**] are the correlations between each pair of variables. Suppose y_i and y_j are two correlated objective functions, the Pearson correlation coefficient $r_{(yi,yj)}$ between them is written as:

$$r_{(y_i;y_j)} = \frac{Cov(y_i, y_j)}{\sqrt{Var(y_i)Var(y_j)}} = \frac{\sum_{i=1}^{n}(y_i - \bar{y}_i)(y_j - \bar{y}_j)}{\sqrt{\left[\sum_{i=1}^{n}(y_i - \bar{y}_i)^2\right]\times\left[\sum_{j=1}^{n}(y_j - \bar{y}_j)^2\right]}} = \frac{\hat{e}_{ij}\sqrt{\hat{\lambda}_i}}{\sqrt{s_{ii}}} \tag{3}$$

Note that $r_{(yi,yj)}$ is directly proportional to the eigenvalues-eigenvectors of [**R]** and its respective covariance.

However, PCA can be derived from the distribution of multivariate normal random variables, $N_p(\boldsymbol{\mu}, \boldsymbol{\Sigma})$. The density of the random variable **Y** is constant on the **μ**-centered ellipsoid such that:

$$(\boldsymbol{y} - \boldsymbol{\mu})' \boldsymbol{\Sigma}^{-1} (\boldsymbol{y} - \boldsymbol{\mu}) = c^2 \qquad (4)$$

Eq. (4) is an ellipse equation centered at the mean vector with half-axes equal to $\pm c\sqrt{\lambda_i} e_i, i = 1, 2, \ldots, p$, where (λ_i, e_i) represents the eigenvalue-eigenvector pairs of **Σ**. In terms of eigenvalues and eigenvectors of covariance matrix, Eq. (4) becomes:

$$\mathbf{y}^{\mathrm{T}}\left[\boldsymbol{\Sigma}_{\mathrm{y}}^{-1}\right]\mathbf{y} = \left(\frac{y_1}{\sqrt{\sigma_{11}}}\right)^2 + \left(\frac{y_2}{\sqrt{\sigma_{22}}}\right)^2 = \mathbf{y}^{\mathrm{T}}\left[\frac{\left(\mathbf{e_1}\mathbf{e_1^{\mathrm{T}}}\right)}{\lambda_1} + \frac{\left(\mathbf{e_2}\mathbf{e_2^{\mathrm{T}}}\right)}{\lambda_2}\right]\mathbf{y} = \frac{\left(\mathbf{y}^{\mathrm{T}}\mathbf{e_1}\right)^2}{\lambda_1} + \frac{\left(\mathbf{y}^{\mathrm{T}}\mathbf{e_2}\right)^2}{\lambda_2} = c^2 \qquad (5)$$

The eigenvectors of variance-covariance or correlation matrices affords the creation of a new set of latent variables called PC scores, by multiplying the matrix of standardized values of the original variables (**Z**), such as $z_{pn} = \left(y_p - \bar{y}_p\right) \times \left(s_{pp}\right)^{-1/2}$, by the matrix of eigenvectors [**P**] such as

$$\boldsymbol{\xi} = \mathbf{P}^{\mathrm{T}}\mathbf{Z} = \begin{bmatrix} e_{11} & e_{12} & \cdots & e_{1p} \\ e_{21} & e_{22} & \cdots & e_{2p} \\ \vdots & \vdots & \ddots & \vdots \\ e_{p1} & e_{2p} & \ldots & e_{pp} \end{bmatrix}^{\mathrm{T}} \times \begin{bmatrix} z_{11} & z_{21} & \cdots & z_{p1} \\ z_{12} & z_{22} & \cdots & z_{p2} \\ \vdots & \vdots & \ddots & \vdots \\ z_{1n} & z_{2n} & \cdots & z_{pn} \end{bmatrix} = \begin{bmatrix} \xi_{11} & \xi_{21} & \cdots & \xi_{p1} \\ \xi_{12} & \xi_{22} & \cdots & \xi_{p2} \\ \vdots & \vdots & \ddots & \vdots \\ \xi_{1n} & \xi_{2n} & \cdots & \xi_{pn} \end{bmatrix} \qquad (6)$$

The PC score relative to the first principal component (PC_1) is the product of an eigenvector and a standardized value of the original variables, given in Eq. (7):

$$PC_{1_1} = \begin{bmatrix} e_{11} & e_{21} & \cdots & e_{p1} \end{bmatrix} \times \begin{bmatrix} z_{11} & z_{21} & \cdots & z_{p1} \end{bmatrix}^{\mathrm{T}} = \sum_{i=1}^{p} e_{1p} z_{1p} \qquad (7)$$

If z_p is a vector of the standardized response of an experimental design, then OLS may be used to create a latent response surface. This hybrid-based (PCA-RSM) approach optimizes multiple correlated responses. For constrained nonlinear optimization problems, the two-fold strategy follows:

$$\begin{cases} \underset{\mathbf{x}\in\Omega}{Min} \quad \hat{f}_p(\mathbf{x}) = \hat{\boldsymbol{\beta}}_p^T \mathbf{z}(\mathbf{x}) = \hat{\beta}_0 + \sum_{i=1}^{k} \hat{\beta}_i x_i + \sum_{i=1}^{k} \hat{\beta}_{ii} x_i^2 + \sum_{i<j}^{k} \sum_{j=2}^{k} \hat{\beta}_{ij} x_i x_j \\ S.t.: \quad g(\mathbf{x}) = \mathbf{x}^{\mathbf{T}}\mathbf{x} - \rho^2 \le 0 \end{cases} \tag{8}$$

where k is the number of factors considered in the experiment, p is the number of responses, $\mathbf{x}^{\mathbf{T}}\mathbf{x} - \rho^2$ represents a hyperspherical experimental region Ω, and $\mathbf{x}^{\mathbf{T}} = [x_1, x_2, \ldots, x_k]$. From Eq. (8), $\mathbf{z}^{\mathbf{T}}(\mathbf{x})$ is defined as:

$$\mathbf{z}^{\mathbf{T}}(\mathbf{x}) = \begin{bmatrix} 1 & x_1 & x_2 & \cdots & x_k & x_1^2 & x_2^2 & \cdots & x_k^2 & x_1x_2 & x_1x_3 & \cdots & x_{(k-1)k1} \end{bmatrix} \tag{9}$$

To keep the prediction variance constant at a given distance ρ from the design center, $\mathbf{x}^{\mathbf{T}}\mathbf{x} - \rho^2 \le 0$ is made equal to $\rho = 2^{(k/4)}$. This property is called "rotatability". For a rotatable central composite design (CCD) with n_c center points, the matrix [**X**] has $n = (2^k + 2k + n_c)$ rows and one column relative to each coefficient of the chosen nonlinear model when Ψ is summed.

This will be considered for the analysis of the PC of many original response surfaces as the number of components required to explain at least 80% explanation of the variance-covariance matrix according to the Kaiser´*s* criteria (Johnson and Wichern, 2007).

The appropriate way of numerically evaluating the accuracy of a multivariate optimization solution in comparison with mathematical solutions is to build a multivariate confidence interval. Suppose there are *p* characteristics, *n* confirmation runs and that the p[th] characteristic is normally distributed as N($\bar{y}_p, s_{pp}$), the 100(1-α)% multivariate confidence interval is given by:

$$\bar{y}_p - \left(\sqrt{\frac{p(n-1)}{n(n-p)} F_{(p,n-p)}(\alpha)} \times \sqrt{\frac{s_{pp}}{n}} \right) \le y_p \le \bar{y}_p + \left(\sqrt{\frac{p(n-1)}{n(n-p)} F_{(p,n-p)}(\alpha)} \times \sqrt{\frac{s_{pp}}{n}} \right) \tag{10}$$

This multivariate confidence interval will be used to represent the results of confirmation tests. The method is effective for finding multiobjective optimization results if the sample mean of these runs falls inside the 100(1-α)% confidence region. Thus, a 2-dimensional confidence ellipse for the mean vector (Johnson and Wichern, 2007) is defined as:

$$\begin{bmatrix} y_1(\mathbf{x}_0) \\ y_2(\mathbf{x}_0^i) \end{bmatrix} = \begin{bmatrix} \bar{y}_1(\mathbf{x}_0) \\ \bar{y}_2(\mathbf{x}_0) \end{bmatrix} + \sqrt{\frac{p(n-1)}{n(n-p)} F_{(p,n-p)}(\alpha)} \times \begin{bmatrix} \sqrt{\lambda_1} & 0 \\ 0 & \sqrt{\lambda_2} \end{bmatrix} \times \begin{bmatrix} e_{11} & e_{12} \\ e_{21} & e_{22} \end{bmatrix} \times \begin{bmatrix} \cos\theta \\ sen\,\theta \end{bmatrix} \tag{11}$$

where $0 \le \theta \le 2\pi$.

3.2. The Normal Boundary Intersection (NBI) method

The NBI method is an optimization approach developed to uniformly spread Pareto frontier for general nonlinear multiobjective problems (Das and Dennis, 1998). It organizes the set of optimal and non-optimal results are organized as a payoff matrix Φ .

The elements of payoff matrix define the Utopia point f^U which represents the minimum value of f_i, and the Nadir point f^N which represents the set of solutions farthest from the optimal solutions. These points allow the normalization of multiple objective functions, such as:

$$\bar{f}_i(\mathbf{x}^*) = \frac{f_i(\mathbf{x}) - f_i^U(\mathbf{x}^*)}{f_i^N(\mathbf{x}^*) - f_i^U(\mathbf{x}^*)} \quad i = 1,\ldots,m \tag{12}$$

where x_i^* is the vector of variables that minimizes the i^{th} objective function $f_i(x)$ individually, $f_i^*(x_i^*)$ is the minimum value of objective function f_i, and $f_p(x_i^*)$ is the value of objective function f_p evaluated on the solution that minimizes the function f_i.

Thus, the payoff matrix is given as:

$$\mathbf{\Phi}_{(p\times p)} = \begin{bmatrix} f_1^*(\mathbf{x_1^*}) & \cdots & f_1(\mathbf{x_i^*}) & \cdots & f_1(\mathbf{x_p^*}) \\ \vdots & \ddots & & & \vdots \\ f_i(\mathbf{x_1^*}) & \cdots & f_i^*(\mathbf{x_i^*}) & \cdots & f_i(\mathbf{x_p^*}) \\ \vdots & & & \ddots & \vdots \\ f_p(\mathbf{x_1^*}) & \cdots & f_p(\mathbf{x_i^*}) & \cdots & f_p^*(\mathbf{x_p^*}) \end{bmatrix} \tag{13}$$

To create a bidimensional evenly distributed Pareto frontier, Eq. (13) was used to execute the following algorithm:

$$\begin{aligned} &\underset{\mathbf{x}\in\Omega}{Min} \;\; \bar{f}_1(\mathbf{x}^*) = \left[\frac{f_1(\mathbf{x}) - f_1^U(\mathbf{x}^*)}{f_1^N(\mathbf{x}^*) - f_1^U(\mathbf{x}^*)}\right] \\ &s.t.: \;\; \left[\frac{f_1(\mathbf{x}) - f_1^U(\mathbf{x}^*)}{f_1^N(\mathbf{x}^*) - f_1^U(\mathbf{x}^*)}\right] - \left[\frac{f_2(\mathbf{x}) - f_2^U(\mathbf{x}^*)}{f_2^N(\mathbf{x}^*) - f_2^U(\mathbf{x}^*)}\right] + 2w_i - 1 = 0 \\ &\qquad g_j(\mathbf{x}) \geq 0; \quad 0 \leq w_i \leq 1 \end{aligned} \tag{14}$$

The optimization problem given by Eq. (8) can then be solved iteratively for different values of w such as $w_p = 1 - \sum_{i=1}^{p} w_i$ (Kovach and Cho, 2009).

3.3. Multivariate Mean Square Error (MMSE)

MMSE transforms the correlated responses into uncorrelated latent variables by attributing the mean to the regression of the PC score, where the i^{th} eigenvalue represents its variance. The

multivariate target of the original response is obtained by multiplying its standardized values by its respective eigenvectors. Using mean square error operator, we have:

$$MMSE_i(x) = \left[\left(PC^i_{x\in\Omega}(x) - \zeta^i_{PC}\right)^2 + \lambda^i_{PC}\right],\ i = 1,2,\dots,(p-r) \tag{15}$$

and

$$\zeta_{PC_i} = \sum_{i=1}^{p}\sum_{p=1}^{\lambda} e_{ip}\left[Z_{ip}\left(Y_{ip}\middle|\zeta_{Y_p}\right)\right] = \sum_{i=1}^{p}\sum_{p=1}^{p} e_{ip}\left[\left(\frac{\overline{Y}_{ip} - \zeta_{Y_p}}{\sigma_{Y_p}}\right)\right] \tag{16}$$

where ζ_{PC} represents the target value of the i^{th} principal components, e_{ip} represents the eigenvector set associated with the i^{th} principal component, and λ_{PC} are eigenvalues associated with each principal component score. If more than one principal component is required, MMSE becomes:

$$MMSE_T = \left\{\prod_{i=1}^{p-r}\left[\left((PC_i - \zeta_{PCi})^2 + \lambda_i|\lambda_i \geq 1\right)\right]\right\}^{\frac{1}{p-r}}\ i = 1,2,\dots,(p-r); r \leq p \tag{17}$$

where $(p-r)$ is the number of significant MMSE functions, and r is the number of principal components discarded by PCA.

The bidimensional form of NBI-MMSE can be obtained by replacing $f_i(\mathbf{x})$ in Eq. (13) by Eq. (15) or (17), where $MMSE_i^U(x) = \min_{x\in\Omega}[MMSE_i(x)]$ and $MMSE_i^N(x)$ is the maximum value defined in the payoff matrix, as a target-based metric that replaces the original variables of the correlated multiresponse dataset, such that:

$$\begin{aligned}
&Min\ \ \bar{f}_1(\mathbf{x}) = \left(\frac{MMSE_1(\mathbf{x}) - MMSE_1^U(\mathbf{x})}{MMSE_1^N(\mathbf{x}) - MMSE_1^U(\mathbf{x})}\right)\\
&s.t.:\ \ g_1(\mathbf{x}) = \left(\frac{MMSE_1(\mathbf{x}) - MMSE_1^U(\mathbf{x})}{MMSE_1^N(\mathbf{x}) - MMSE_1^U(\mathbf{x})}\right) - \left(\frac{MMSE_2(\mathbf{x}) - MMSE_2^U(\mathbf{x})}{MMSE_2^N(\mathbf{x}) - MMSE_2^U(\mathbf{x})}\right) + 2w - 1 = 0\\
&g_2(\mathbf{x}) = \mathbf{x}^{\mathrm{T}}\mathbf{x} \leq \rho
\end{aligned} \tag{18}$$

Note that correlated responses are not withdrawn from the multiresponse dataset by PCA. Fig. 2 illustrates the difference between correlated responses and linear dependencies. Although all linear dependencies present significant correlations, not every pair of response variables are linearly dependent.

The functions $f_1(\mathbf{x})$ and $f_2(\mathbf{x})$ are linearly dependent and have the same stationary point while $f_3(\mathbf{x})$ and $f_4(\mathbf{x})$ have different anchor points which define the Utopia line. In manufacturing fields, cutting time and overall machining time are practical examples of functions $f_1(\mathbf{x})$ and

$f_2(\mathbf{x})$ respectively. They are distinguished by a single constant called “unproductive time”, which corresponds to the time wasted in advance and the retreat of the machining tool in each pass. Therefore, it is not necessary to consider both objective functions in the same multiobjective problem.

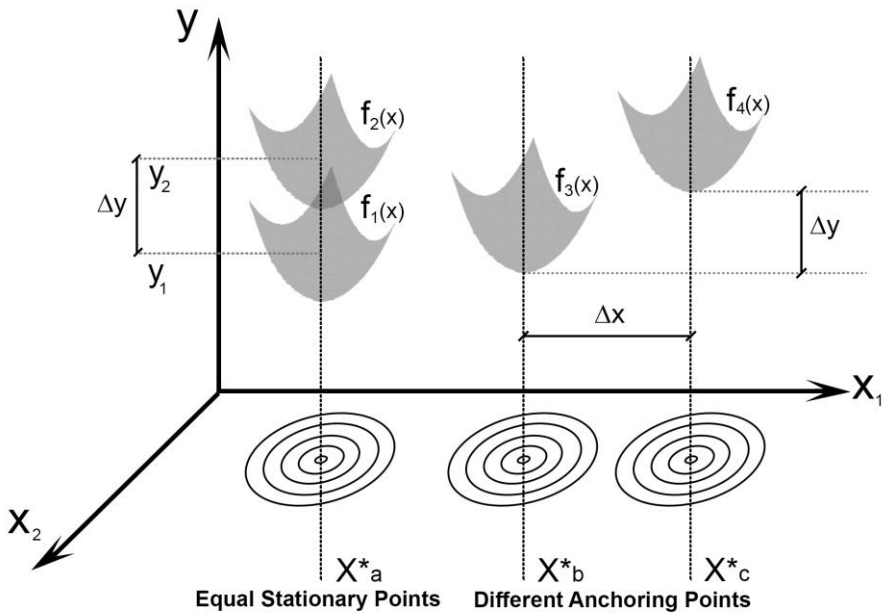

Figure 2: Difference between linear dependencies and correlations in multiresponse data.

3.5. Pareto frontier quality and best solution

The Pareto frontier contains all the non-dominated and feasible solutions for correlated multiresponse data. However, some solutions are better than others. According to Ahmadi *et al.* (2012), Ahmadi *et al.* (2015), and Aghaei *et al.* (2011), the best solution is found using a linear membership for each objective function based a fuzzy criterion, such that:

$$\mu_i = \begin{cases} 1 & MMSE_i \leq MMSE_i^U \\ \dfrac{MMSE_i^N - MMSE_i}{MMSE_i^N - MMSE_i^U} & MMSE_i^U < MMSE_i < MMSE_i^N \\ 0 & MMSE_i \geq MMSE_i^N \end{cases} \tag{19}$$

where $MMSE_i^U$ and $MMSE_i^N$ are Utopia and Nadir points respectively. Eq. (19) shows the extent at which a non-dominated solution satisfies the $MMSE_i$ objective. The total membership function (or fuzzy decision maker index (FDM)) may be evaluated based on the individual membership functions and the relative importance of objective functions (w_i) as:

$$\mu^T = \sum_{n=1}^{k} w_i \, \mu_i \tag{20}$$

where the highest value of μ^T indicates the best solution.

Rocha *et al*., 2015 proposed a multiobjective target-based metric based on each optimized value, the targets defined to the original variables to create the also called Global Percentage Error index (GPE). The GPE of optimized responses evaluates the distance between the point and the target and is given by:

$$GPE = \sum_{i=1}^{m} \left| \frac{y_i^*}{T_i} - 1 \right| \tag{21}$$

where y_i^* is the value of the optimized responses, T_i is the i[th] target, and m is the number of objective functions considered.

However, GPE only focuses on few objective functions while leaving more difficult objectives with null weights. Therefore, Shannon's entropy index (S(w)), (Rocha *et al*., 2016; Rocha *et al*., 2017) is employed for better diversification of the weights (w_i) and is given by:

$$S(w) = -\sum_{i=1}^{m} w_i \ln(w_i) \tag{22}$$

Note that GPE is a minimization index type while S(w) is a maximization type. In other words, the vector that maximizes Eq. (22) has an equal solution of $w_i = 1/m$. However, this vector does not guarantee solutions close to the targets. Hence it cannot be used as the sole decision parameter. However, Rocha *et al*. (2016) proposed the maximization of the ratio of S(w) and GPE such that:

$$SE_{Ratio} = \sum_{i=1}^{m} \frac{-w_i \ln(w_i)}{\left| \frac{y_i^*}{T_i} - 1 \right|} \tag{23}$$

The Entropy-Error ratio (SE_{Ratio}) was used to appraise the overall performance of NBI-MMSE, NNC, AHL, NBI and desirability methods in this research.

4. Results and discussion

4.1. AISI H13 hardened steel turning process using PCBN 7025 tool

In this section, we present a numerical illustration of NBI-MMSE approach applied to the multiobjective optimization of AISI H13 hardened steel turning process. A PCBN CB 7025 (CNGA 120408 S01030A) tool with TiC coverage (Sandvik Coromant, Sandviken, Sweden) was used in the turning of AISI H13 hardened steel of hardness 54 HRC, until a wear of 0.3 mm was made, to prevent the tool from breaking (Fig. 3). The experiments were conducted on a MHP Kingsbury turning center with 18 kW spindle motor, 4-4500 RPM speed range, 12-

station tool turret, and 200 mm plate diameter, which is available at the Machining Laboratory of the Department of Mechanical Engineering in the University of Aveiro, Portugal. This process was done using the steps outlined in Fig. 1.

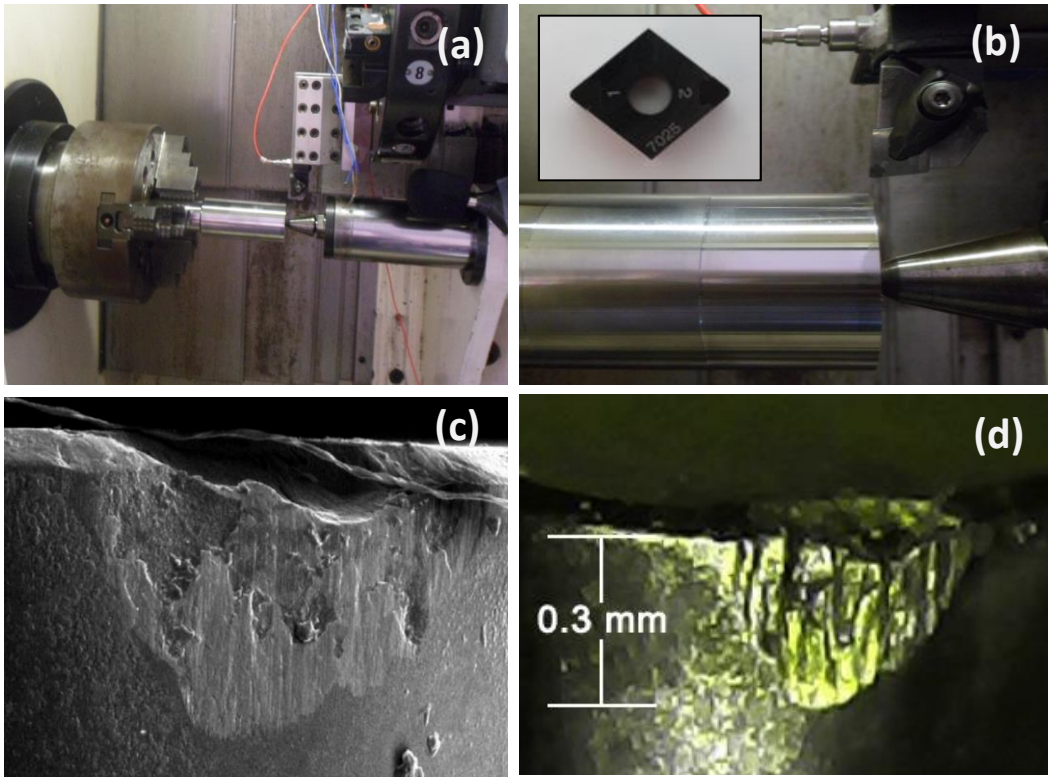

Figure 3: (a) AISI H13 turning, (b) Insertion of PCBN-7025, (c) tool wear captured by Scanning Electron Microscope (SEM-200X), and (d) 20X magnification for VBmax=0.3 mm.

Fonte: Campos (2015) - coauthor.

Step 1: A sequence of 19 experiments were conducted using a CCD with three parameters at two levels ($2^k = 2^3 = 8$), six axial points (2k = 6), five center points, and axial distance of 1.682. Table 1 shows the parameters and respective levels while Table 2 presents the experimental design of the respective responses.

Table 1. Control variables and work levels

Control Variables	Symbol	Work levels				
		-1.682	-1	0	1	1.682
Cutting speed (m/min)	V_c	57.39	100	162.5	225	267.61
Cutting feed (mm/rev)	f	0.06	0.10	0.16	0.225	0.24
Machining depth (mm)	A_p	0.09	0.15	0.225	0.33	0.39

The multiple responses of AISI H13-PCBN 7025 include tool life (T), machining total cost (K_p), surface roughness (R_a), machining force (F_r), sound pressure level (SPL), and the specific cutting energy (SCE).

Table 2. Experimental data of the experimental procedure

Run	Inputs			Outputs					
	V_c (m/min)	f (mm/rev)	A_p *(mm)*	T (min)	K_p (U$)	R_a (μm)	F_r (N)	SPL (dB)	SCE (cm^3/N.min)
1	100.00	0.10	0.15	66.00	3.66	0.62	346.87	67.35	$4.36x10^{-3}$
2	225.00	0.10	0.15	33.00	2.33	0.64	242.23	89.50	$1.41x10^{-2}$
3	100.00	0.22	0.15	54.00	3.47	2.14	438.69	74.49	$7.71x10^{-3}$
4	225.00	0.22	0.15	30.00	2.17	2.15	247.78	90.93	$3.08x10^{-2}$
5	100.00	0.10	0.33	63.00	5.20	0.65	460.97	68.57	$7.36x10^{-3}$
6	225.00	0.10	0.33	31.50	3.01	0.62	244.27	91.87	$2.99x10^{-2}$
7	100.00	0.22	0.33	53.00	4.61	1.93	458.47	74.77	$1.61x10^{-2}$
8	225.00	0.22	0.33	31.50	1.79	2.39	251.65	92.29	$6.66x10^{-2}$
9	57.39	0.16	0.24	60.50	5.51	0.67	498.39	79.83	$4.54x10^{-3}$
10	267.61	0.16	0.24	25.50	1.87	1.17	229.99	99.27	$4.57x10^{-2}$
11	162.50	0.05	0.24	40.00	4.32	0.31	330.76	83.52	$6.78x10^{-3}$
12	162.50	0.26	0.24	41.50	2.58	2.14	365.33	85.87	$2.86x10^{-2}$
13	162.50	0.16	0.09	51.50	2.28	1.20	336.28	84.59	$6.97x10^{-3}$
14	162.50	0.16	0.39	48.50	3.46	0.70	368.76	85.66	$2.80x10^{-2}$
15	162.50	0.16	0.24	43.50	3.47	0.81	343.84	86.49	$1.86x10^{-2}$
16	162.50	0.16	0.24	44.50	3.42	0.82	342.92	83.91	$1.87x10^{-2}$
17	162.50	0.16	0.24	42.50	3.53	0.83	341.33	84.77	$1.87x10^{-2}$
18	162.50	0.16	0.24	43.25	3.41	0.81	340.28	85.84	$1.86x10^{-2}$
19	162.50	0.16	0.24	44.00	3.36	0.83	343.76	86.59	$1.88x10^{-2}$
Mean (u_{Y_i})				44.59	3.34	1.13	343.82	84.01	$1.42x10^{-2}$
Standard deviation (σ_{Y_i})				11.46	1.05	0.66	78.88	8.08	$1.61x10^{-2}$
Utopia point (ξ_i)				24.90	2.62	0.28	230.28	96.39	$2.12x10^{-2}$
Standardized $Z(Y_i \mid \xi_{Y_i})$				-1.19	-1.62	-1.29	-1.36	1.16	0.041

Each response characteristic was measured by an optical microscope (Mitutoyo TM-500) with 30X magnification and 1 μm resolution, and a Scanning Electron Microscope (SEM/200X), which enabled the tool's cutting edges to flank wear measurements, as shown in Fig. 3. A maximum tool flank wear of Vb_{max}=0.3 mm characterized the end of tool life, which is the time needed to reach this maximum wear. Fig. 4a shows the tool life curves for each of the 19 experiments of rotatable CCD. It was observed that tool life increased as cutting speed decreased. Moreover, there was a common pattern in the curves characterized by a positive relationship between tool wear and life.

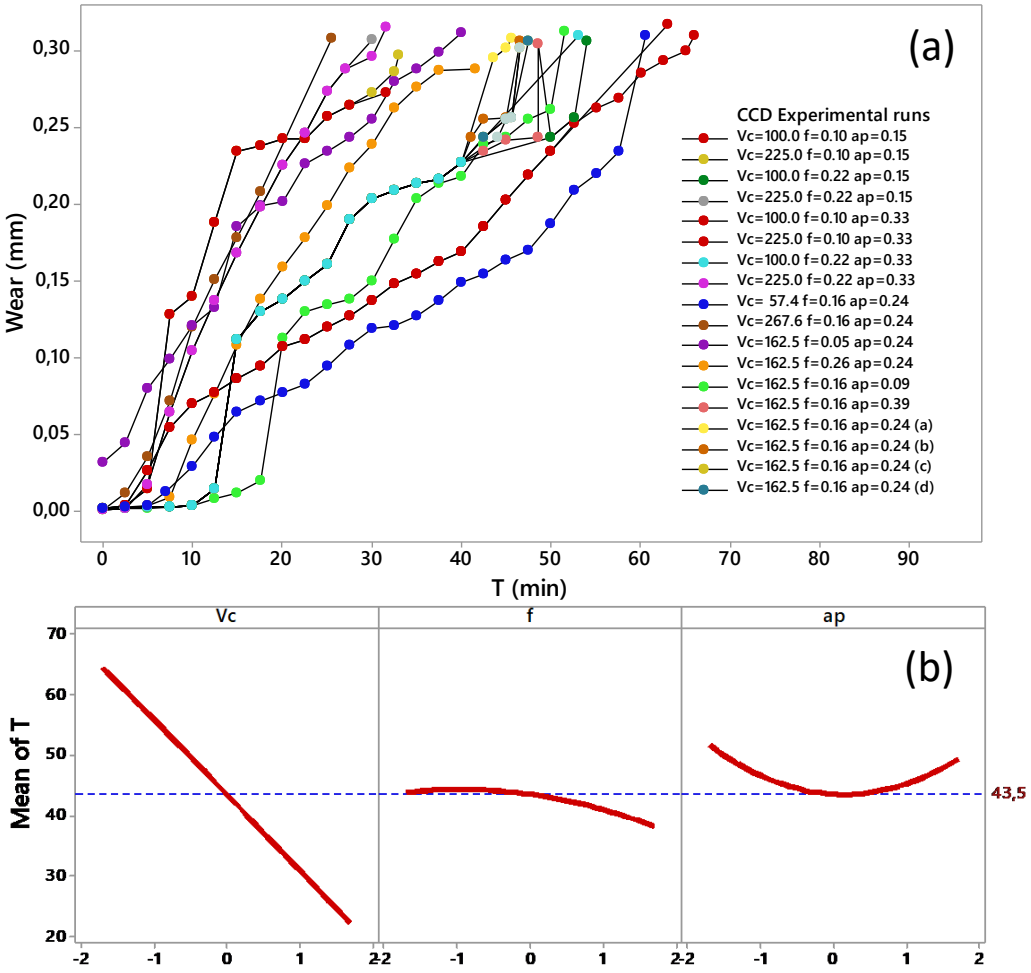

Figure 4: (a) PCBN 7025 tool life curves, (b) Influence of input factors on tool life.

Fig. 4b highlights the influence of V_c, f, and A_p on T. Statistical analysis revealed that V_c and f were significant in explaining the linear variation of tool life, while A_p was only significant as a quadratic effect. The interaction between V_c and f was also significant at α=5%. The full quadratic model (Table 3) for T had adjusted R-squared (R^2adj) value of 93%.

The wear rate for PCBN 7025 shown in Fig. 5 describes the relationship between tool life and wear. When the angular coefficient of each tool wear curve represented in Fig. 4a was correlated with the respective cumulative cutting time, the wear rate decreased considerably as speed increased. However, the process productivity ($MRR=V_c{}^{*}f^{*}A_p$) was also reduced since the material removal rate was diminished, which is undesirable. A negative (and significant) Pearson´s correlation coefficient of r=-0.92 was then found for this pair of variables. This relationship pattern exemplifies how conflicts between objective functions are common in manufacturing processes and underlines the importance of solving them, as proposed in this work.

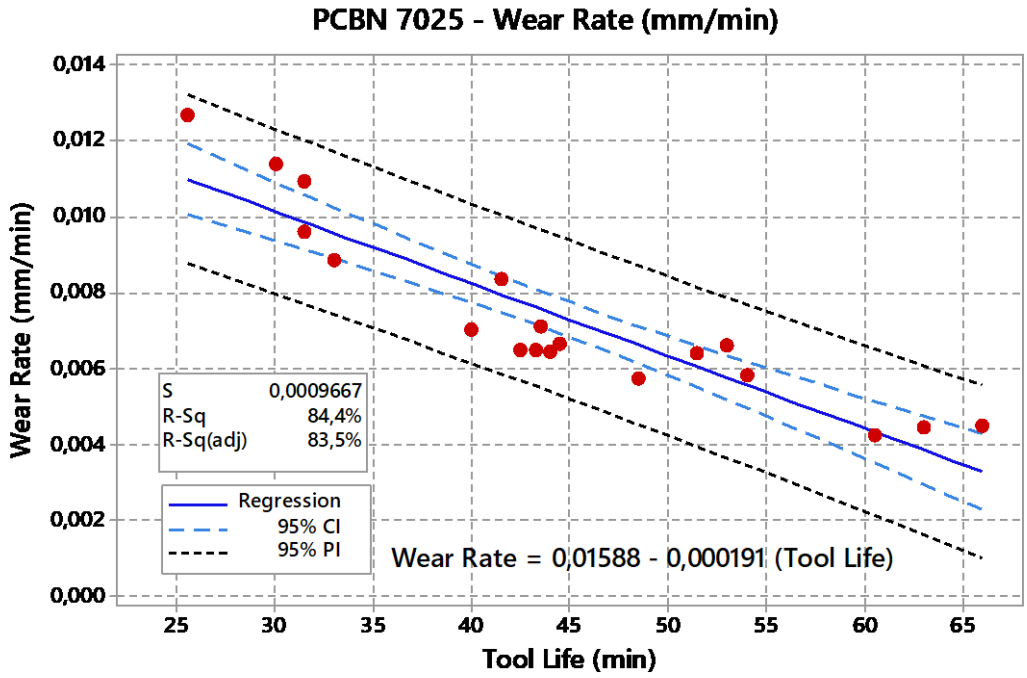

Figure 5: PCBN 7025 tool life curves.

Proceeding with the experimental framework, a Hommeltester T-1000 needle roughness meter furnished the surface roughness (R_a) data presented in Table 2. A Kistler 9121 piezoelectric dynamometer coupled with a Kistler 5019 load amplifier and its respective data acquisition system (Dynoware Software Data Acquisition) allowed the machining force (F_r) measurements for each CCD experimental condition described in Table 2. A dynamometer with RS232 interface and a software Dynoware Kistler allowed the data acquisition in real time.

SCE is the ratio between MRR of each experiment and its respective F_r. Therefore, there should be a significant correlation between F_r and SCE. The SPL is obtained by a 3200B shock accelerometer (Dytran Instruments, Inc) and a 4102C signal conditioner (Dytran Instruments, Inc) directly from the vibration process measurement. The experiment was interfaced with a computer using a BNC-2120 connector block (National Instruments Corporation) and a PCI-643 I/O card (National Instruments Corporation). Moreover, the data was obtained a rate of 1 kHz (highest rotation: 300 rpm) using LabVIEW® software. Finally, signal noise removal was done by a wavelet transform, using MATLAB® software to improve its accuracy.

The multiresponse data presented in Table 2 was processed by OLS to find the coefficients of the full quadratic models for each response of interest. The models had high values of R^2adj and normally distributed residuals. Table 3 shows these results.

Table 3. Full quadratic models of original responses of AISI H13 hardened steel turning.

β	**Model**	**T (min)**	**K_p (U$)**	**R_a (μm)**	**F_r (N)**	**SPL (dB)**	**SCE (cm^3/N.min)**	**z(x)**
β_0	Constant	43.527	3.440	0.807	343.174	85.725	1.86×10^{-2}	1
β_1	*Vc*	-12.365	-1.008	0.095	-85.705	8.209	1.28×10^{-2}	x_1
β_2	*f*	-1.646	-0.372	0.671	11.744	1.402	7.48×10^{-3}	x_2
β_3	*D*	-0.662	0.364	-0.059	14.236	0.515	7.20×10^{-3}	x_3
β_{11}	Vc^2	-0.066	0.078	0.110	3.577	0.296	2.69×10^{-3}	x_1^2
β_{22}	f^2	-0.861	-0.007	0.217	-2.131	-1.420	6.19×10^{-5}	x_2^2
β_{33}	d^2	2.409	-0.212	0.120	-0.549	-1.268	-1.06×10^{-5}	x_3^2
β_{12}	*Vc x f*	2.375	-0.075	0.060	-9.549	-1.436	5.16×10^{-3}	x_1x_2
β_{13}	*Vc x d*	0.500	-0.298	0.050	-15.996	0.279	5.03×10^{-3}	x_1x_3
β_{23}	*f x d*	0.625	-0.183	0.002	-11.561	-0.244	3.17×10^{-3}	x_2x_3
R^2 (%)		96.47	98.29	91.36	97.40	86.64	98.62	
R^2adj. (%)		92.95	96.58	82.72	94.79	73.28	97.25	$\hat{f}_p(\mathbf{x}) = \hat{\boldsymbol{\beta}}_p^T \mathbf{z}(\mathbf{x})$
AD (P-Value)*		0.540	0.089	0.909	0.417	0.243	0.095	

*P-Value of Anderson-Darling Normality Test (P-Value<5%, then the residuals from $f_p(\mathbf{x})$ are normal).

Step 2: Correlations among the several responses were computed. Table 4 shows the results among the response pairs.

Table 4. Pearson's Correlation coefficient between each pair of the original RSM-CCD responses.

	T	K_p	R_a	F_r	SPL
K_p	0.738 **0.000**[1]				(symmetrical)
R_a	-0.217 0.372	-0.426 0.069			
F_r	0.851 **0.000**	0.842 **0.000**	-0.038 0.876		
SPL	-0.926 **0.000**	-0.718 **0.001**	0.120 0.626	-0.776 **0.000**	
SCE	-0.737 **0.000**	-0.666 **0.002**	0.482 **0.037**	-0.655 **0.002**	0.709 **0.001**

(1)Values in bold indicate the significance of correlation when P-Value < 0.05.

The correlation is significant if the P-value (values in bold) is less than the significance level (α=5%). However, R_a did not have any significant correlation while the other responses had high levels of correlation to a considerable degree of interdependence capable of supporting the PCA framework. This correlation pattern affords the transformation of the functions into clusters based on their similarity.

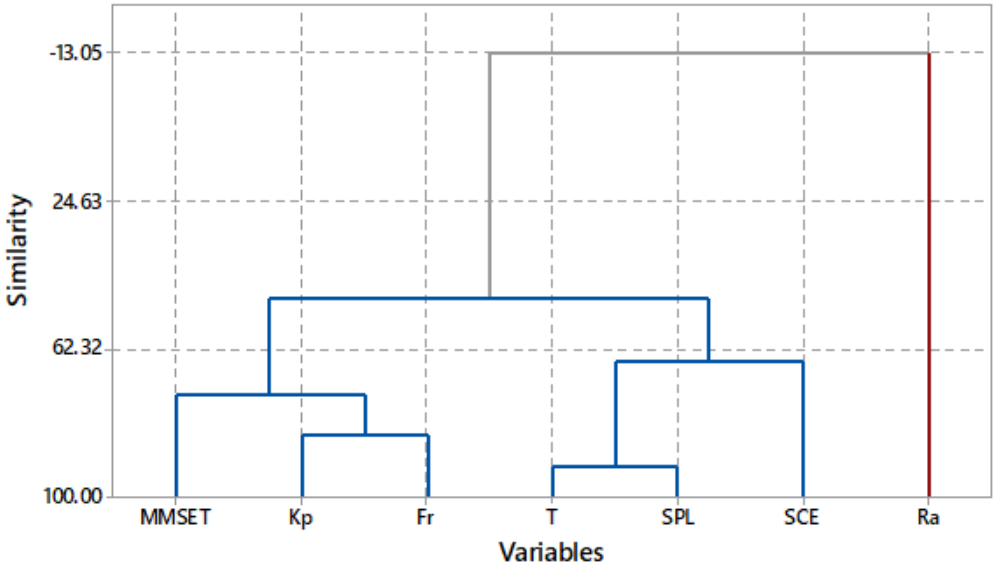

Figure 6: Hierarchical Cluster Analysis. Cluster 1: K_p, F_r, T, SPL, SCE; Cluster 2: R_a

Fig. 6 shows the formation of two clusters: Cluster 1 (T, K_p, F_r, SPL, SCE) and Cluster 2 (R_a). However, $MMSE_T$ may be added to the hierarchical cluster analysis (HCA) to replace all responses for comparison with the R_a of a bidimensional Pareto frontier.

Step 3: An eigen analysis was applied to the multiresponse data. However, R_a was removed from PCA because it did not have any significant correlation. The results of the eigen analysis and PC scores of AISI turning process of Cluster 1 variables are shown in Table 5. The first two PCs explain 87.3% of the overall variation present in matrix [**Y**]. As PC_1 and PC_2 were orthogonal, they were considered as independent responses. Fig. 7 shows the relationships between PC_1 and standardized responses. The objective functions built with PC scores show a similar behavior and also establish the orthogonality between PC_1 and PC_2.

Applying OLS algorithm to PC_1 and PC_2 (Table 5), the multivariate full quadratic models are:

$$PC_1 = 0.009 - 2.241V_c - 0.410f + 0.002a_p - 0.078V_c^2 + 0.008f^2 + 0.057a_p^2 - 0.036V_cf - 0.340V_ca_p - 0.168fa_p \quad (24)$$

$$PC_2 = 0.109 + 0.073V_c - 0.241f - 0.576a_p - 0.261V_c^2 - 0.001f^2 + 0.110a_p^2 - 0.087V_cf + 0.003V_ca_p + 0.049fa_p \quad (25)$$

These models had R^2adj. values above 80.00%, indicating that the response surfaces are adequate. Figure 8 shows the response surface for PC_1 and PC_2 as a function of all input parameters.

Table 5. Eigen analysis of correlated responses observed on AISI H13 turning process and PC scores.

PCA Eigenanalysis					
	PC_1	**PC_2**	**PC_3**	**PC_4**	**PC_5**
Eigenvalue	3.376	0.989	0.392	0.183	0.060
Proportion	0.675	0.198	0.078	0.037	0.012
Cumulative	0.675	0.873	0.951	0.988	1.000
Eigenvectors					
	e_{1p}	**e_{2p}**	**e_{3p}**	**e_{4p}**	**e_{6p}**
T	0.528	-0.023	0.143	-0.230	0.804
Kp	0.177	-0.940	-0.177	0.229	-0.046
Fr	0.481	0.138	0.580	0.594	-0.245
SPL	-0.516	0.046	-0.036	0.665	0.537
SCE	-0.438	-0.309	0.781	-0.316	0.050

Principal Component Scores

Run	**Z_1(T)**	**Z_2(Kp)**	**Z_3(Fr)**	**Z_4(SPL)**	**Z_5(SCE)**	**PC_1**	**PC_2**
1	1.8675	0.3064	0.0387	-2.0622	-1.0391	2.4045	0.8738
2	-1.0112	-0.9649	-1.2878	0.6803	-0.4218	-1.6296	1.2264
3	0.8207	0.1248	1.2027	-1.1782	-0.8227	1.8658	0.1489
4	-1.2729	-1.1178	-1.2175	0.8573	0.6521	-2.3059	0.3618
5	1.6058	1.7783	1.4851	-1.9112	-0.8570	3.4433	-0.4636
6	-1.1421	-0.3149	-1.2620	0.9737	0.6360	-1.9583	0.1131
7	0.7335	1.2144	1.4534	-1.1435	-0.2765	2.1802	-0.7841
8	-1.1421	-1.4810	-1.1684	1.0257	2.9483	-3.3914	-1.4143
9	1.3877	2.0746	1.9595	-0.5170	-1.0285	3.1150	-0.7577
10	-1.6655	-1.4045	-1.4430	1.8899	1.5986	-3.5793	-0.2824
11	-0.4006	0.9372	-0.1656	-0.0601	-0.8822	0.5336	0.4821
12	-0.2697	-0.7259	0.2727	0.2308	0.5185	-0.6392	-0.3189
13	0.6026	-1.0127	-0.0956	0.0723	-0.8698	0.1156	1.0849
14	0.3409	0.1152	0.3162	0.2048	0.4836	0.0650	-0.5980
15	-0.0953	0.1248	0.0003	0.3076	-0.1328	-0.0775	0.0413
16	-0.0080	0.0770	-0.0114	-0.0119	-0.1296	0.0829	0.0853
17	-0.1825	0.1821	-0.0316	0.0946	-0.1241	-0.0136	0.0471
18	-0.1171	0.0674	-0.0449	0.2271	-0.1204	-0.1016	0.0784
19	-0.0517	0.0196	-0.0008	0.3200	-0.1325	-0.1095	0.0760
e_1^T	0.4721	0.4398	0.4552	-0.4599	-0.4061	$PC_1 = \sum_{i=1}^{p} (e_{1p} z_p)$	
e_2^T	-0.0058	-0.3396	-0.4697	-0.0795	-0.8110	$PC_2 = \sum_{i=1}^{p} (e_{2p} z_p)$	

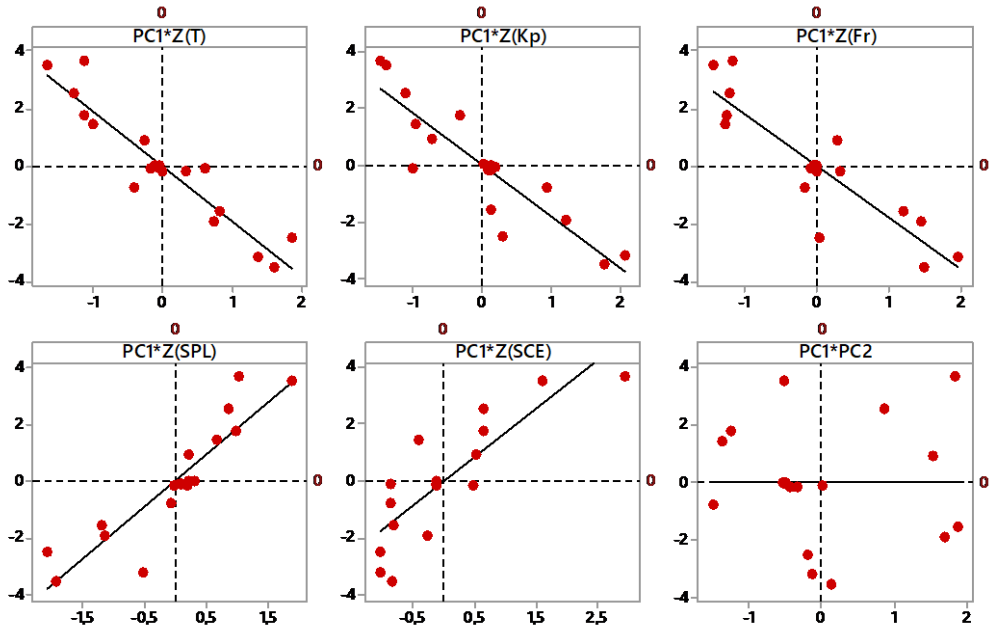

Figure 7: Regression equations between PC_1 and standardized responses.

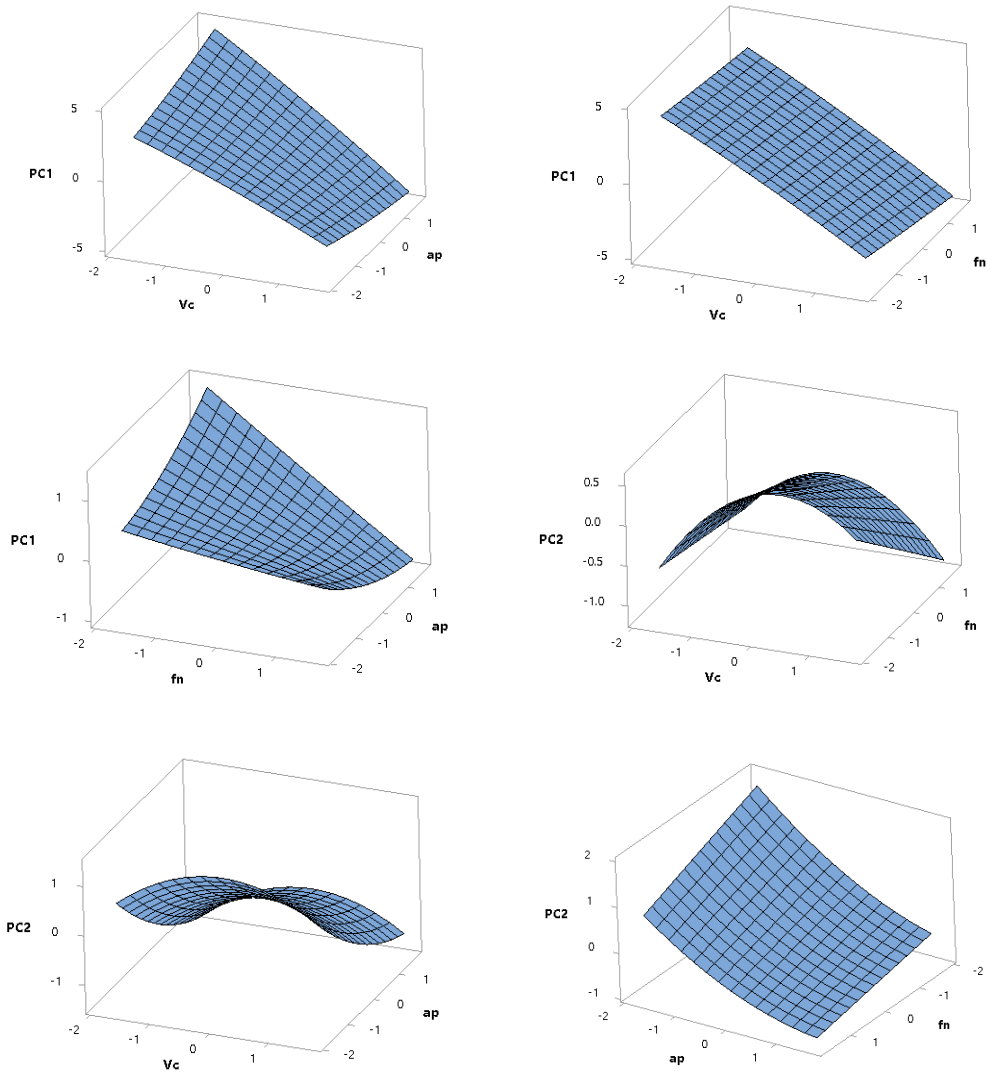

Figure 8: Response surfaces built based on process parameters.

Step 4: The individual optimization of the original responses and of the PCs were implemented using the coefficients obtained by the algorithm. R_a, T and SCE were minimized while K_p, F_r, and SPL were minimized. The results of individual optimization, described as Utopia points, are detailed in Table 2 above. PC_1 and PC_2 eigenvectors show that it is not possible to optimize all responses simultaneously from Eq. (24) and (25), since some objective functions exhibit different optimization directions. Therefore, the MMSE method is more appropriate since it is capable of transforming the optimization directions of all objective functions to the minimization of a mean squared error. Accordingly, $MMSE_T$ objective function will be minimized.

Step 5: The payoff matrix of Eq. (26) was formed by minimizing both $MMSE_T$ and R_a. Its elements (Utopia and Nadir points) were used to normalize the objective functions to avoid undesirable optimization consequences due to differences of scale. For AISI H13-PCBN 7025, the payoff matrix for $MMSE_T$ and R_a is:

$$\Phi = \begin{bmatrix} 1.321 & 2.835 \\ 0.959 & 0.281 \end{bmatrix} \tag{26}$$

Step 6: The matrix in Eqn. (26) was used to normalize the objective functions based on Eq. (1) for bivariate optimization to give:

$$\bar{f}(x) = \begin{cases} \overline{MMSE}_T = \dfrac{MMSE_T(x) - 1.321}{2.835 - 1.321} \\ \\ \bar{R}_a = \dfrac{R_a(x) - 0.281}{0.959 - 0.281} \end{cases} \tag{27}$$

Step 7: NBI-MMSE optimization using GRG algorithm was applied to solve Eq. (18), where the nonlinear constraint refers to the experimental region. Since all objective functions were obtained based on the experimental points of the hypersphere of radius ρ, only solutions falling within this region are considered feasible. In this study, $\rho = \sqrt[4]{2^3} = 1.682$, for three input variables. Therefore, the equation of the experimental region is $\mathbf{x}^{\mathbf{T}}\mathbf{x} - \rho^2 = \mathbf{x}^{\mathbf{T}}\mathbf{x} - (1.682)^2$ or $\mathbf{x}^{\mathbf{T}}\mathbf{x} \leq 2.829$.

Weights in the range [0:1] and with the increments of 5% were used to construct the Pareto frontier with 21 optimal points as shown in Fig. 9. The optimization results are shown in Table 5.

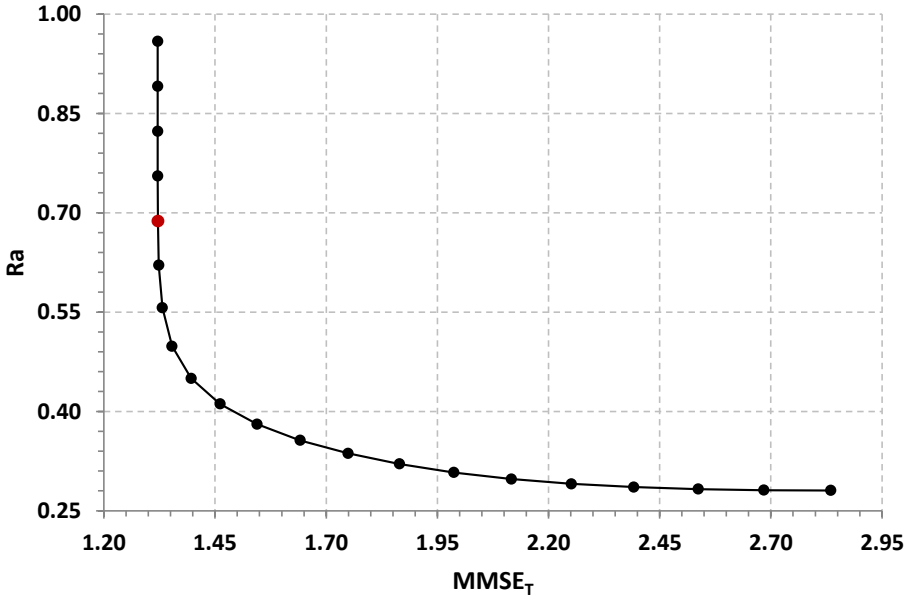

Figure 9: Pareto frontier of R_a vs $MMSE_T$ obtained by NBI-MMSE method.

Table 6. Pareto optimal solutions for NBI-MMSE approach

	Uncoded Units			**Outputs (Y_p)**						**Frontier results**	
w1	V_c *(m/min)*	*f (mm/rev)*	*Ap (mm)*	T *(min)*	K_p *(U$)*	R_a *(μm)*	F_r *(N)*	SPL *(dB)*	SCE *(cm³/N.min)*	$MMSE_T$	Fuzzy
0.00	157.63	0.07	0.26	45.0	4.23	0.28	334.9	79.6	0.75	28.35	0.0100
0.05	161.49	0.07	0.26	44.0	4.16	0.28	328.8	80.2	0.77	26.85	0.1083
0.10	165.94	0.07	0.26	42.9	4.08	0.28	322.3	80.8	0.79	25.37	0.2051
0.15	170.96	0.06	0.26	41.6	3.99	0.29	315.3	81.6	0.83	23.92	0.2997
0.20	176.67	0.06	0.25	40.2	3.89	0.29	307.8	82.5	0.87	22.52	0.3914
0.25	182.99	0.06	0.25	38.6	3.79	0.30	300.1	83.6	0.94	21.16	0.4797
0.30	189.70	0.06	0.25	36.9	3.69	0.31	292.3	84.8	1.01	19.87	0.5639
0.35	196.59	0.07	0.25	35.1	3.59	0.32	284.7	86.0	1.11	18.65	0.6439
0.40	203.60	0.07	0.25	33.4	3.49	0.34	277.0	87.3	1.21	17.49	0.7194
0.45	210.09	0.07	0.25	31.8	3.38	0.36	270.0	88.6	1.35	16.41	0.7894
0.50	216.60	0.07	0.24	30.4	3.26	0.38	263.0	89.9	1.49	15.45	0.8525
0.55	223.15	0.08	0.24	28.9	3.13	0.41	255.9	91.3	1.65	14.61	0.9065
0.60	229.66	0.08	0.23	27.6	3.00	0.45	248.9	92.6	1.81	13.96	0.9485
0.65	235.71	0.09	0.22	26.6	2.86	0.50	242.3	93.8	1.96	13.53	0.9758
0.70	240.61	0.09	0.21	26.0	2.72	0.56	237.2	94.7	2.07	13.32	0.9892
0.75	243.99	0.10	0.20	25.9	2.59	0.62	234.1	95.3	2.14	13.23	0.9935
0.80	**246.05**	**0.11**	**0.19**	**26.1**	**2.49**	**0.69**	**232.7**	**95.6**	**2.20**	**13.22**	**0.9939**
0.85	246.85	0.12	0.18	26.6	2.40	0.76	232.8	95.7	2.24	13.21	0.9930
0.90	246.72	0.12	0.17	27.2	2.33	0.82	234.0	95.6	2.27	13.20	0.9920
0.95	246.73	0.13	0.16	27.7	2.26	0.89	235.1	95.5	2.30	13.19	0.9910
1.00	246.83	0.14	0.16	28.2	2.20	0.96	236.1	95.3	2.33	13.18	0.9900

Note: The values in bold represent the optimal point obtained through the Fuzzy Decision Maker. Specific cutting energy (SCE) was written in terms of a 10^{-2} power.

Fig. 10 shows the overlaid contour plots built for response surfaces based on each parameter. These plots show the complexity of AISI H13 turning and illustrate that NBI-MMSE was capable of generating a Pareto frontier inside the extremely-constrained feasible region.

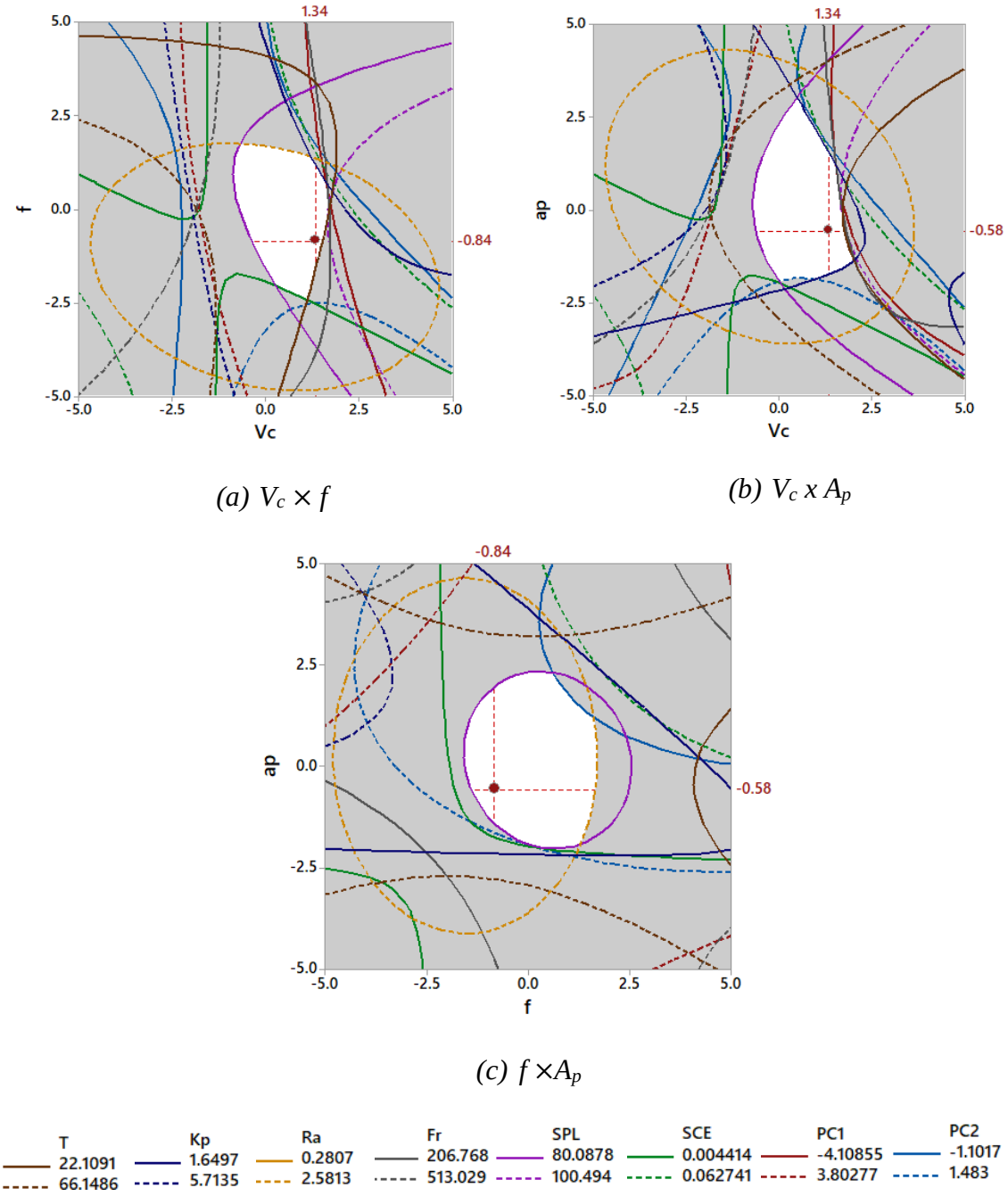

Figure 10: Overlaid contour plot with the process optimal solution.

Step 8: The fuzzy criteria was used to identify the best solution for the AISI H13 hardened steel turning process with multiobjective optimization. A fuzzy decision maker was used to decide the best solution among the 21 Pareto points. The weighting factors considered in this problem have the following importance: w_1= 0.99 for $MMSE_T$ objective function and w_2 = 0.01 for R_a. If the $MMSE_T$ objective function represents five original responses, its process importance is

higher. Thus, the maximization of μ^T described in Eq. (20) was done to obtain the optimal weight for each objective function. The results are presented in Table 6. The best solution obtained by NBI-MMSE (in bold typeface) has the highest value of total membership (μ^T = 0.9939) and represents 80% of $MMSE_T$ (Cluster 1) and 20% of R_a (Cluster 2).

Step 9: The power and sample size capabilities were evaluated before designing and running confirmation experiments, to ensure that they are sufficient to detect differences of magnitude between the selected optimal points for T, K_p, R_a, F_r, SPL, and SCE using NBI-MMSE approach.

Then, T was used to determine the sample size for the experimental responses at a confidence level of 95%. Afterwards, a one-sample t-test was done to confirm whether the optimal value obtained for T through the proposed algorithm of optimization falls within the multivariate confidence interval. The t-test can detect the difference of at least one pass in the turning machine at 80% power, as shown in Fig. 11. Using a pre-test value of 0.6 as standard deviation, the sample size was 10. However, this sample size value was also used for the remaining responses. Thus, a series of 10 experiments conducted for NBI-MMSE approach under optimal experimental conditions produced the following results: V_c = 246 m/min, f = 0.11 mm/rev, and A_p = 0.19mm. Ten different tool edges were used to machine n=10 workpieces until a flank tool wear of ~0.3 mm was achieved. Table 7 shows the confirmation results for NBI-MMSE approach. All sample means fall within the 95% multivariate confidence interval with sample mean values very close to the predicted values.

The upper and lower bounds of the mean values (Table 7) for 95% multivariate confidence interval are based on Eq. (10), with p=6, n=10, $F_{(p,n-p)}(\alpha) = F_{(6,4)}(0.05) = 6.2$ for sample mean $\bar{y}_p$ and variance s_{pp} respectively. For these confirmation experiments, T (highlighted in red bullets on Fig. 11) was ~26 min for a maximal allowable tool wear of 0.3 mm and MRR=5.14 cm^3/min. Moreover, K_p was ~US$ 2.50 per piece. Fig. 12 and 13 are snapshots from the third confirmation experiment.

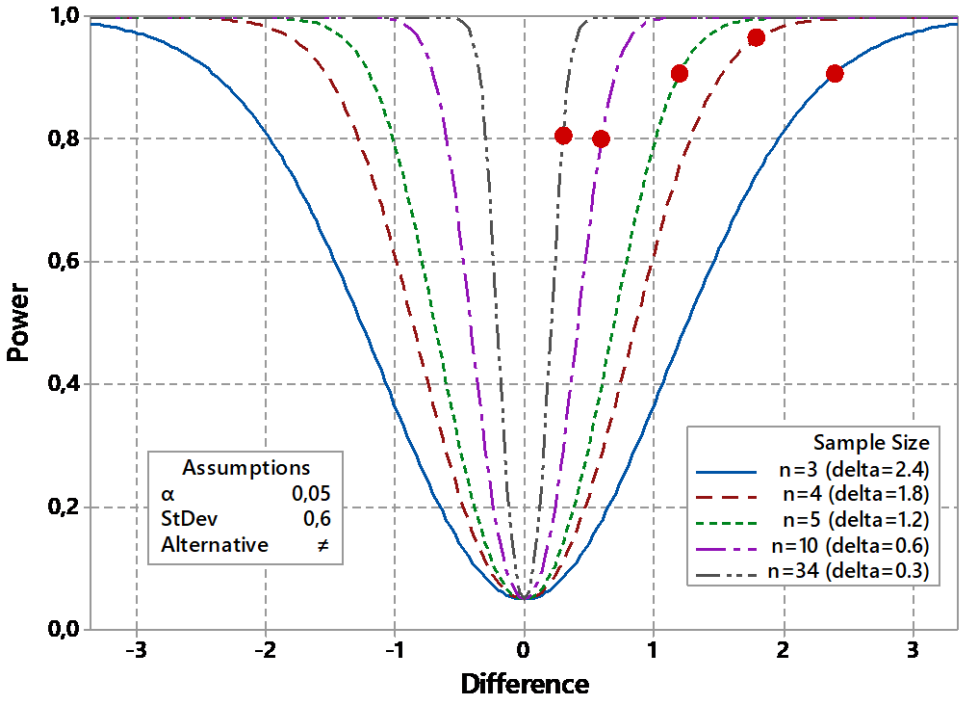

Figure 11: Sample size calculation for confirmation runs (power =80%; α=5%; σ=0.6 min)

Table 7. Confirmation runs for NBI-MMSE method at w=0.8 for AISI H13-PCBN 7025 turning.

n	T (min)	K_p (U$)	R_a (µm)	F_r (N)	SPL (dB)	SCE (cm^3/N.min)
1	26.30	2.552	0.67	232.78	95.50	2.209 x10^{-2}
2	25.30	2.245	0.74	230.38	95.84	2.276 x10^{-2}
3	**26.20**	**2.525**	**0.68**	**233.20**	**95.80**	**2.186 x10^{-2}**
4	26.78	2.590	0.65	235.60	96.00	2.299 x10^{-2}
5	26.80	2.723	0.63	237.40	95.06	2.168 x10^{-2}
6	25.60	2.350	0.72	230.41	95.83	2.276 x10^{-2}
7	26.20	2.522	0.66	234.18	95.08	2.170 x10^{-2}
8	25.60	2.356	0.72	230.20	95.87	2.281 x10^{-2}
9	26.30	2.512	0.67	232.60	95.80	2.171 x10^{-2}
10	26.10	2.510	0.69	233.44	95.60	2.191 x10^{-2}
Mean	**26.118**	**2.489**	**0.683**	**233.019**	**95.637**	**2.223 x10^{-2}**
SD	0.493	0.137	0.035	2.343	0.331	5.361 x10^{-4}
Error:	1.56x10^{-1}	4.34x10^{-2}	1.10x10^{-2}	7.42x10^{-1}	1.05x10^{-1}	1.70 x10^{-4}
(1)CI UB:	26.274	2.532	0.694	233.761	95.742	2.24x10^{-2}
Pareto:	**26.075**	**2.487**	**0.688**	**232.652**	**95.608**	**2.20**x10^{-2}
(2)CI LB:	25.962	2.445	0.671	232.277	95.532	2.21x10^{-2}

(1)CI UB: Multivariate upper bound for confidence interval; (2)CI LB: Lower bound.

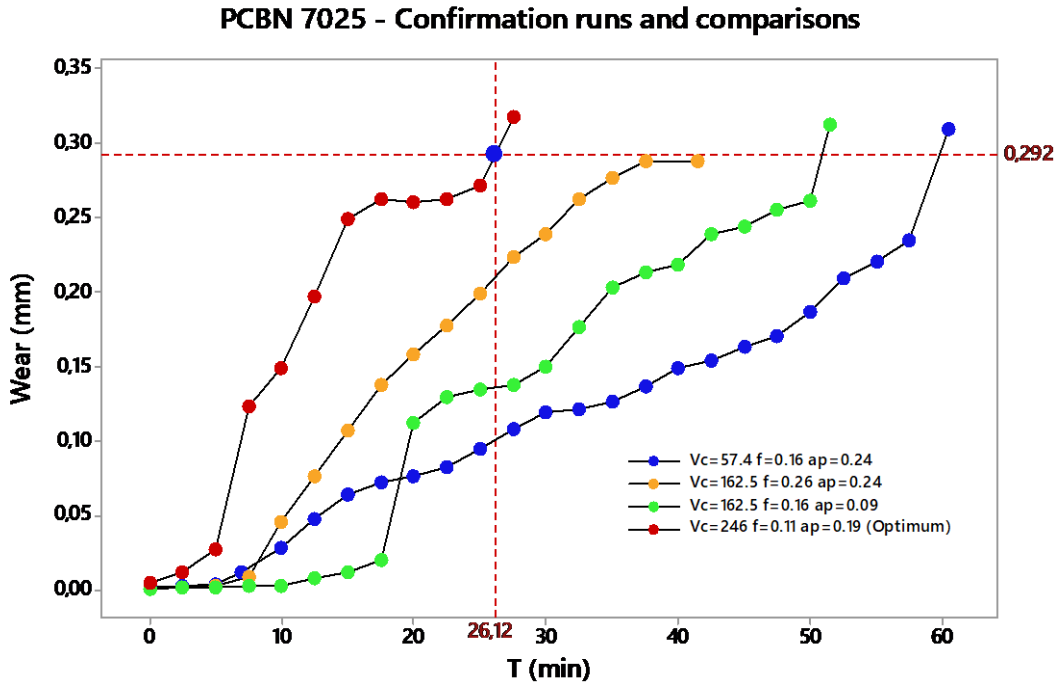

Figure 12: Confirmation runs for tool wear and tool life (VBmax≈0.30 mm).

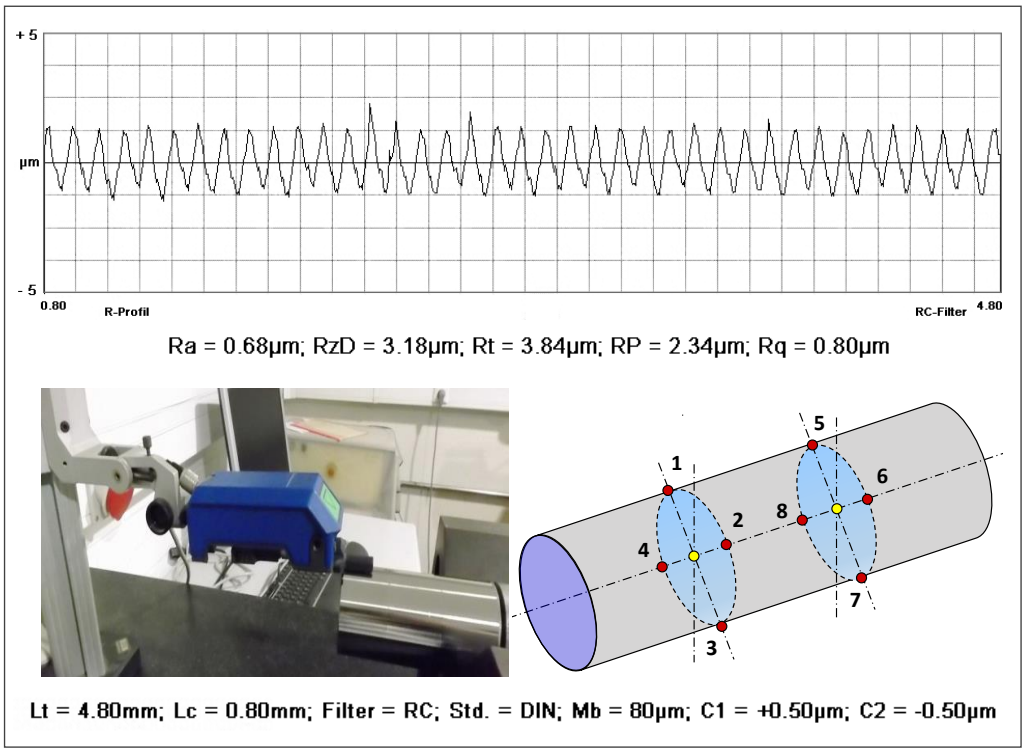

Figure 13: – PCBN 7025: Confirmation runs for Surface Roughness

R_a was measured at four points of the workpiece phased at 90º near the live center and near the center of the workpiece. Moreover, ten measurements of F_r and SPL were made during the tests. The mean values of these measurements are reported on Table 7.

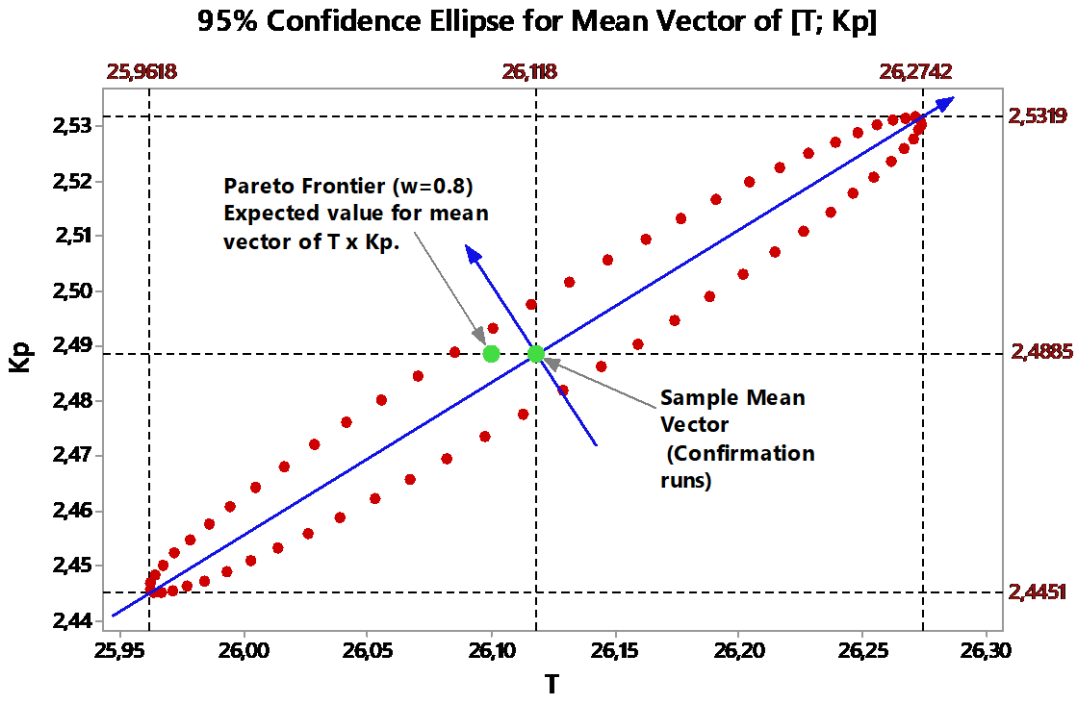

Figure 14: 95% Confidence ellipse for K_p vs T

Finally, a 95% bidimensional confidence ellipse for T and K_p was plotted (Fig. 14) to verify whether the confirmation runs have similar correlations with the original dataset. However, the bidimensional vector of the confirmation runs for these two responses falls within the confidence ellipse, thereby confirming the accuracy of the representation of correlated response by their respective PC_1 and PC_2 values.

4.2. Benchmark test functions

The case study considered employed the experimental data of six correlated objective functions. Therefore, to test if some aspects of NBI-MMSE methodology may be useful for general cases, we will use six correlated benchmark test functions. These functions are generally used to test the ability of an algorithm to escape from any local minimum and to evaluate its performance. If the exploration process of an algorithm is poorly designed, then it cannot search the function landscape effectively, thereby subjecting the algorithm to a local minimum.

Before solving an optimization problem, it is important verify the aspects of the function landscape that make the optimization process difficult. Then, benchmark functions can be classified in terms of their dimensionality once the problem difficulty and the number of objective functions increase (Jamil and Yang, 2013). The exponential increase in number of dimensions may be a significant barrier for the most optimization algorithms for highly non-linear problems.

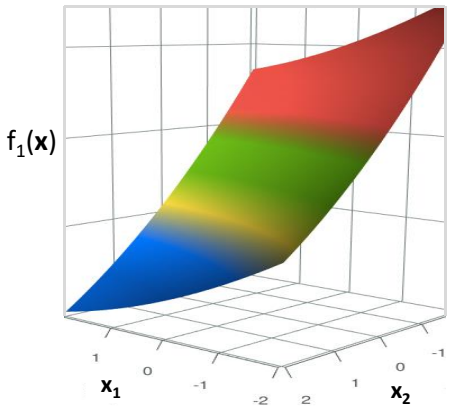

$$f_1(x_1, x_2) = (0.111x_1^2 + 0.0625x_2^2 - 1.333x_1 - 0.500x_2 + 4.999)$$

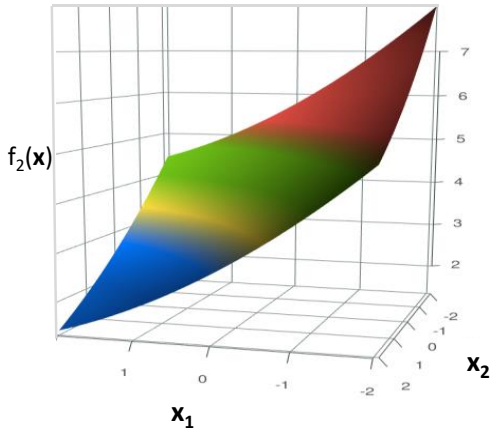

$$f_2(x_1, x_2) = (0.0625x_1^2 + 0.1111x_2^2 - 0.7500x_1 - 0.8888x_2 + 4.0276)$$

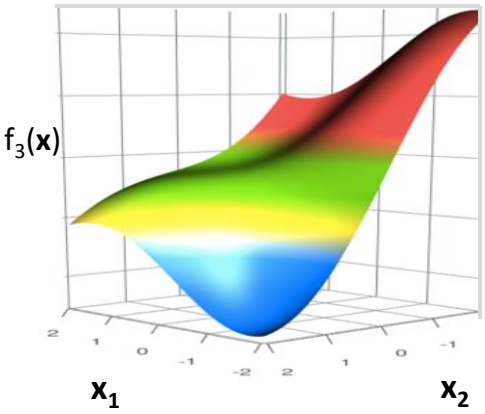

$$f_3(x_1, x_2) = (0.111x_1^2 - 1.555x_1 + 5.443) + sin(x_1)sin(x_2)(0.0204x_2^2 - 0.2040x_2 + 1.51)$$

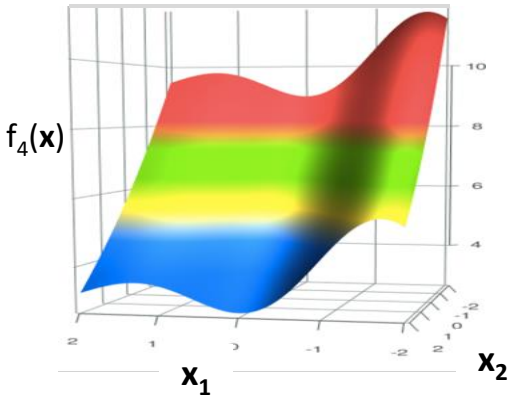

$$f_4(x_1, x_2) = 0.111x_1^2 - 1.555x_1 + 5.444 + sin^2(x_2)(0.0625x_2^2 - 0.625x_2 + 1.562)$$

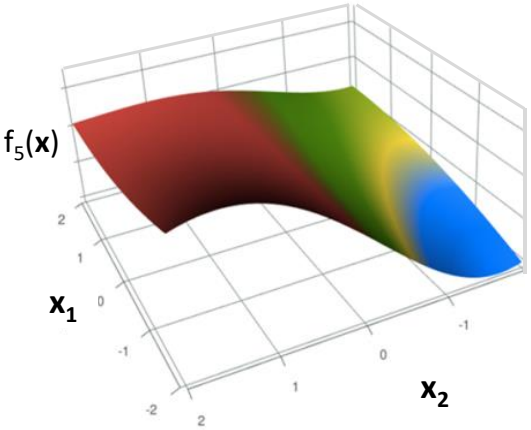

$$f_5(x_1, x_2) = sin(x_1)(0.0123x_1^2 + 0.0400x_2^2 - -0.0984x_1 - 0.1600x_2 + 0.3568)$$

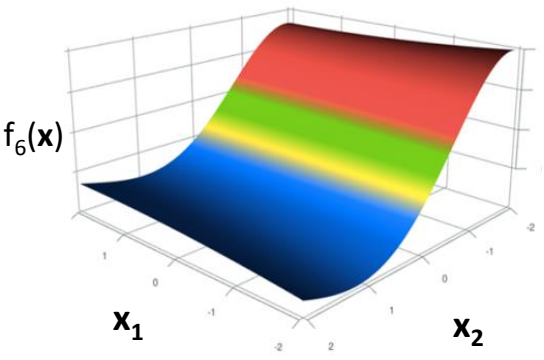

$$f_5(x_1, x_2) = sin(x_1)(0.0123x_1^2 + 0.0400x_2^2 - 0.0984x_1 - 0.1600x_2 + 0.3568)$$

Figure 15: Benchmark test functions.

Thus, the benchmark functions used in this study is a collection of six continuous, non-separable, unimodal and correlated test functions described in Fig. 15. Table 8 presents simulated results of the functions based on CCD.

Table 8. Test functions response through input variables of CCD and PC scores

Input variables		f_1	f_2	f_3	f_4	f_5	f_6	**PC_1C_1**	**PC_1C_2**
x_1	**x_2**								
-1.000	-1.000	7.0007	5.840	7.631	8.704	-0.563	0.935	2.955	2.900
1.000	-1.000	4.340	4.340	3.480	5.593	0.396	-0.396	-0.466	-2.442
-1.000	1.000	6.007	4.063	6.880	7.819	-0.293	0.852	1.056	1.906
1.000	1.000	3.340	2.563	4.231	4.708	0.127	-0.313	-2.364	-1.447
-1.414	0.000	7.108	5.213	7.867	7.867	-0.516	1.207	2.316	3.206
1.414	0.000	3.337	3.092	3.467	3.467	0.240	-0.313	-2.521	-2.016
0.000	-1.414	5.832	5.507	5.444	7.953	0.000	0.000	1.877	-0.301
0.000	1.414	4.418	2.993	5.444	6.229	0.000	0.000	-0.986	-0.301
0.000	0.000	5.000	4.028	5.444	5.444	0.000	0.000	-0.373	-0.301
0.000	0.000	5.000	4.028	5.444	5.444	0.000	0.000	-0.373	-0.301
0.000	0.000	5.000	4.028	5.444	5.444	0.000	0.000	-0.373	-0.301
0.000	0.000	5.000	4.028	5.444	5.444	0.000	0.000	-0.373	-0.301
0.000	0.000	5.000	4.028	5.444	5.444	0.000	0.000	-0.373	-0.301

The six functions were highly correlated as shown in Table 9. Hence, the PCs were able to reduce the problem's dimensionality by neutralizing the correlation effects. PC_1 of Cluster 1 explains 90.40% of the variance-covariance matrix obtained from f_1, f_2, and f_4 which were replaced by their respective PC scores. In the same vein, PC_1 of Cluster 2 explains 97.40% of the variance-covariance matrix obtained from f_3, f_5, and f_6 which were replaced by their respective PC scores.

Table 9. Correlation between the tests functions *(*pvalue)*

	f_1	f_2	f_3	f_4	f_5
f_2	0.872 0.000*				
f_3	0.923 0.000*	0.634 0.020*			
f_4	0.902 0.000*	0.795 0.001*	0.827 0.000*		
f_5	-0.880 0.000*	-0.604 0.029*	-0.977 0.000*	-0.791 0.001*	
f_6	0.894 0.000*	0.613 0.026*	0.949 0.000*	0.805 0.001*	-0.959 0.000*

After the PCs were obtained and stored, OLS algorithm was applied to obtain the second order models of the PC scores as shown in the following equations.

$$PC_1C_1 = -0.374 - 1.710x_1 - 0.981x_2 + 0.167x_1^2 + 0.440x_2^2 - 1.825.10^{-16}x_1x_2 \quad (28)$$

$$PC_1C_2 = -0.301 - 2.010x_1 - 2.741.10^{-17}x_2 + 0.469x_1^2 + 0.021x_2^2 + 0.497x_1x_2 \quad (29)$$

The optimization of individual functions were done sequentially using GRG algorithm, thereby obtaining the minimum value of each function. MMSE method was used to minimize the six functions simultaneously, with their respective targets expressed in terms of PCs. Hence, two equations of MMSE were obtained: $MMSE_1$ and $MMSE_2$. Using the NBI optimization approach, the payoff matrix was created, thereby obtaining the individual optimizations of $MMSE_i$ objective functions and the Utopia and Nadir points given by:

$$\emptyset = \begin{bmatrix} 2.733 & 8.740 \\ 4.981 & 2.923 \end{bmatrix} \quad (30)$$

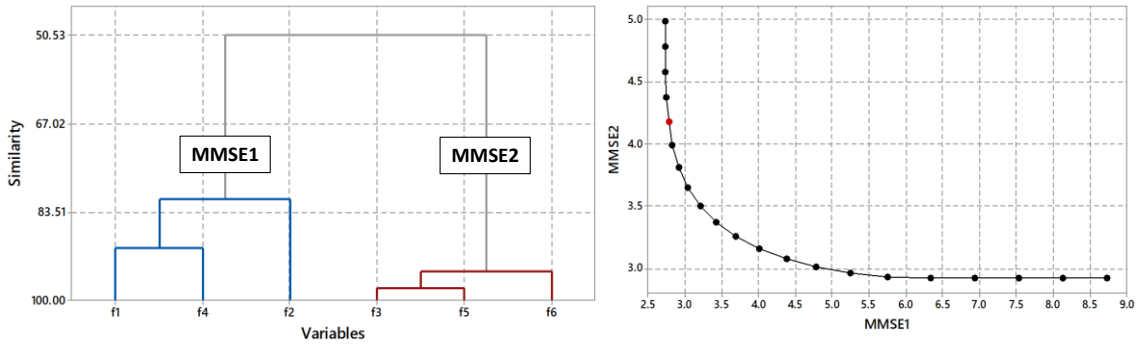

(a) (b)

Figure 16: (a) Hierarchical Cluster Analysis, and (b) NBI-MMSE Pareto frontier.

Using the matrix $\emptyset$ in Eq. (30), the objective functions based on Eq. (1) was obtained for bivariate optimization problems. Afterwards, GRG algorithm was applied on the system described in Eq. (18). The nonlinear constraint in this case was $x^T x \leq 1.999$ which corresponds to the axial distance of 1.414 determined by the CCD. Several weights (w) ranging from [0:1] and with increments of 5% were adopted to construct the Pareto frontier with 21 optimal points shown in Table 10 and Fig. 16(b). Thus, NBI-MMSE approach generates a convex and equidistant Pareto frontier.

A fuzzy decision maker was used to discover the best result of the Pareto frontier by setting the importance of the weighting factors at w_1= 0.92 and w_2 = 0.08. The best solution obtained by NBI-MMSE approach is indicated in Table 10 (in bold typeface) with the highest value of total membership (μ^T= 0.943).

Table 10. Pareto-optimal solutions for NBI-MMSE approach from tests functions

w_1	Input		Benchmarking test functions						Pareto Frontier		Fuzzy
	x_1	x_2	f_1	f_2	f_3	f_4	f_5	f_6	$MMSE_1$	$MMSE_2$	
0.00	0.022	0.000	4.97	4.01	5.41	5.41	0.007	-0.013	8.74	2.92	0.080
0.05	0.023	0.135	4.90	3.89	5.41	5.35	0.007	-0.013	8.14	2.92	0.172
0.10	0.025	0.299	4.82	3.75	5.41	5.33	0.006	-0.013	7.54	2.92	0.264
0.15	0.029	0.516	4.72	3.58	5.40	5.37	0.006	-0.013	6.94	2.92	0.356
0.20	0.039	0.886	4.56	3.30	5.40	5.63	0.004	-0.012	6.34	2.92	0.448
0.25	0.127	1.289	4.29	2.97	5.30	6.08	0.010	-0.044	5.76	2.93	0.536
0.30	0.233	1.395	4.12	2.83	5.19	6.12	0.017	-0.087	5.25	2.96	0.613
0.35	0.323	1.377	4.01	2.78	5.10	5.95	0.025	-0.123	4.79	3.01	0.681
0.40	0.414	1.352	3.91	2.73	5.00	5.78	0.032	-0.156	4.38	3.08	0.741
0.45	0.506	1.320	3.80	2.68	4.90	5.59	0.040	-0.186	4.02	3.16	0.794
0.50	0.599	1.281	3.70	2.65	4.80	5.39	0.048	-0.213	3.70	3.26	0.839
0.55	0.693	1.233	3.61	2.61	4.69	5.19	0.057	-0.237	3.43	3.37	0.875
0.60	0.787	1.175	3.52	2.59	4.58	4.97	0.066	-0.257	3.21	3.50	0.904
0.65	0.878	1.108	3.44	2.57	4.47	4.76	0.077	-0.274	3.04	3.65	0.925
0.70	0.966	1.033	3.37	2.56	4.35	4.54	0.090	-0.288	2.92	3.81	0.937
0.75	1.046	0.952	3.31	2.57	4.24	4.35	0.103	-0.299	2.84	3.99	0.943
0.80	**1.117**	**0.867**	**3.26**	**2.58**	**4.13**	**4.17**	**0.118**	**-0.307**	**2.79**	**4.18**	**0.943**
0.85	1.179	0.781	3.23	2.60	4.03	4.02	0.134	-0.313	2.76	4.37	0.939
0.90	1.231	0.695	3.21	2.64	3.93	3.89	0.150	-0.318	2.74	4.57	0.934
0.95	1.275	0.612	3.20	2.67	3.84	3.79	0.166	-0.322	2.74	4.78	0.928
1.00	1.311	0.529	3.20	2.71	3.76	3.71	0.182	-0.326	2.73	4.98	0.920

Note: The values in bold represent the optimal point obtained through the Fuzzy Decision Maker.

5. Comparison with other optimization algorithms

To evaluate the application of NBI-MMSE, we compared its results with other algorithms. We used a mixed-methods strategy to generate equidistant Pareto frontiers for NBI-MMSE and for the optimizations of the original functions. NNC and AHL methods were considered in the first group, using R_a and $MMSE_T$ as the first and second functions respectively. They were then determined using the same steps in Fig. 1. The details of the AHL and NNC methods are beyond the scope of this work. However, there are several recent works on AHL (Schatz *et al*., 2017, Pereyra *et al*., 2013) and NNC (Pereira *et al*., 2017; Gobbi *et al*., 2014; Messac *et al*., 2003; Messac and Mattson, 2002) methods.

Fig. 17 shows the Pareto frontiers of R_a vs $MMSE_T$ for NNC and AHL using NBI. The results were consistent with each other. Thus, it is difficult to determine the most suitable method. However, the best values of each frontier were chosen to compose the results presented in Table 11. The best Pareto point for NBI-MMSE was the vector [$w(R_a)$=0.2; $w(MMSE_T)$=0.8].

The NBI-MMSE results were then compared with GCM given by:

$$\begin{aligned} &\underset{\mathrm{X}\in\Omega}{Min}\ \ \bar{f}(\mathbf{x}) = \sum_{i=1}^{m} w_i \left[\frac{f_i(\mathbf{x}) - f^U}{f_i^U} \right]^2 \\ &S.t.:\ \ \mathbf{x}^{\mathrm{T}}\mathbf{x} \le \rho^2 \end{aligned} \tag{31}$$

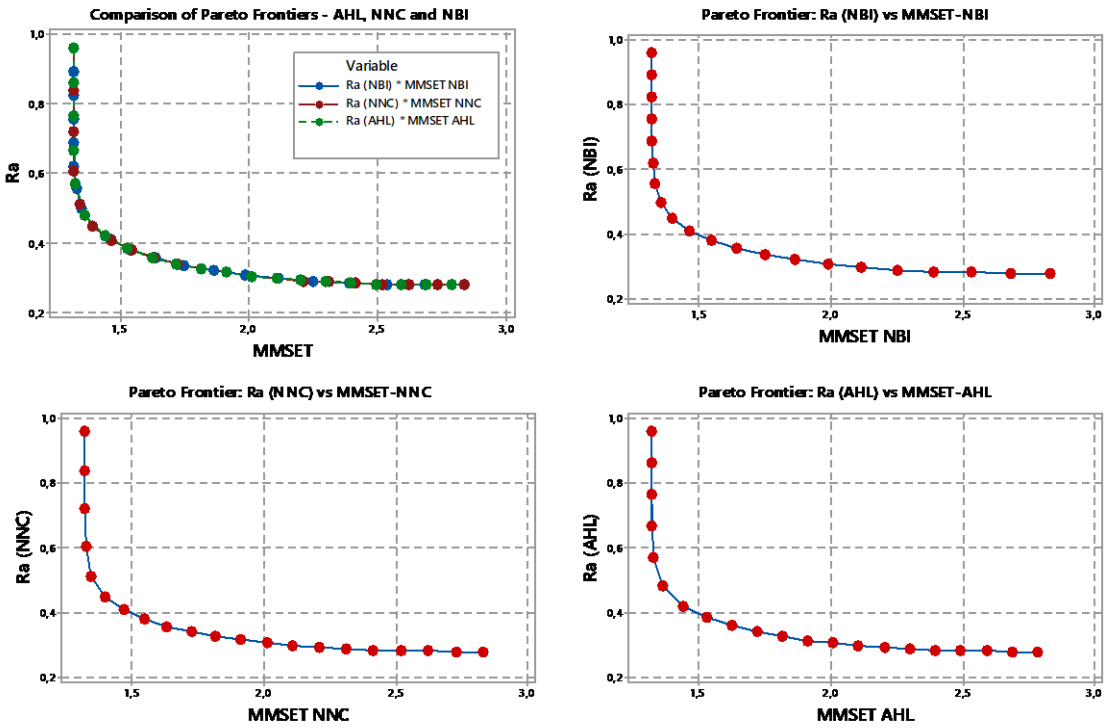

Figure 17: Pareto frontier of R_a vs $MMSE_T$ obtained by MMSE using NBI method

Recall that $MMSE_T$ had a weight $w(MMSE_T)=0.8$ for the best solution and represented five responses. If this weight was shared with the original outputs, each one would receive a weight of 16%. However, when GCM was designed using $\mathbf{w}_{(a)}^{T} = [0.16\ \ 0.16\ \ 0.20\ \ 0.16\ \ 0.16\ \ 0.16]$, similar results were obtained. Therefore, different solutions were obtained when compared with the targets, as shown in Table 11. In other words, the methods were not congruent.

Table 11. Comparisons among several multiobjective optimization methods.

MOP Method	**T**	**K_p**	**R_a**	**F_r**	**SPL**	**SCE**
NBI-MMSE	26.080	2.490	0.690	232.670	95.610	2.200
GCM^1	33.854	2.532	0.614	250.639	89.814	0.757
GCM^2	25.099	2.674	0.588	234.150	95.654	1.988
Target:	**24.900**	**2.620**	**0.700**	**230.300**	**96.390**	**2.120**

GCM^1: obtained with same weights of NBI-MMSE; GCM^2: obtained with Simplex Lattice design.

On the other hand, a mesh with 259 weight vectors was created based on simplex-lattice mixture design {3;6} (Montgomery, 2009) to exploit the optimization region and determine a better setup for GCM. For each weight vector from simplex-lattice design, GCM was run iteratively to determine the distances from the original targets (GPE). Fig. 17 illustrates these results and highlights the GPE performance for the largest entropy vector $\mathbf{w}_{(a)}^{T}$ and $\mathbf{w}_{(b)}^{T} = [0.6\ \ 0.0\ \ 0.0\ \ 0.0\ \ 0.0\ \ 0.4]$, whose results were the closest to the targets. Fig. 17(a) is a

subregion of the entire simplex space shown by Fig. 18(b). It is interesting that the best solution with GCM was reached with null weights for K_p, R_a, F_r, and SPL.

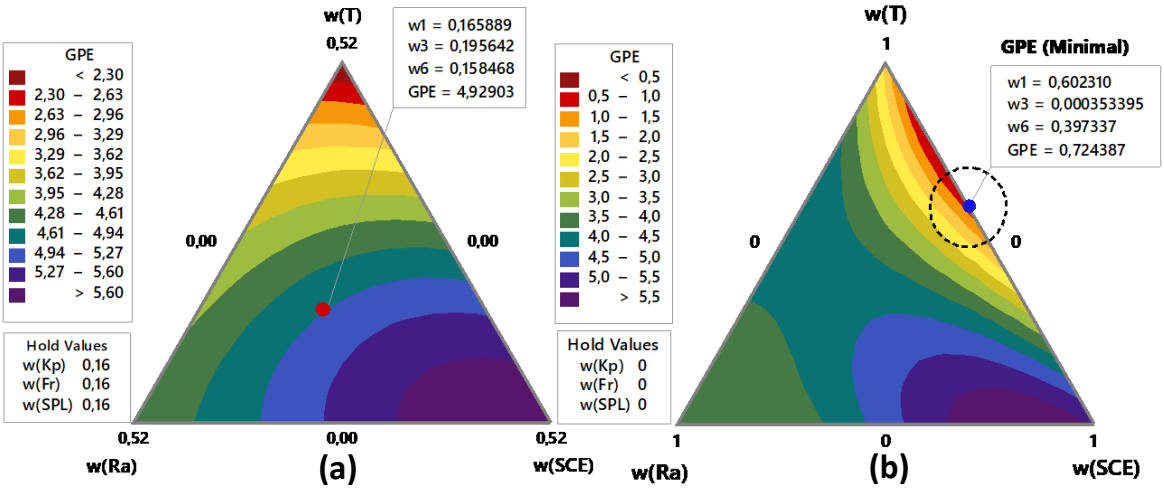

Figure 18: GPE gradient for GCM method for $\boldsymbol{w}^T_{(a)}$ and $\boldsymbol{w}^T_{(b)}$.

Furthermore, desirability method was compared with a "nominal-is-the-best" transformation using the same targets as in the other trials (Fig. 19).

On a first attempt, the center point was used as a feasible initial solution (starting value), but the results were not suitable. Therefore, the same optimum of NBI-MMSE for w=0.8 was used instead, but it was not able to converge to feasible solutions (Fig. 19a). After several attempts to adjust the optimization parameters of the desirability method using NBI-MMSE configurations, the feasible solution was found as shown in Fig. 19b.

Table 12 summarizes the results of the comparison of NBI-MMSE, NBI, AHL, NNC, GCM and desirability based on some criteria: minimal global percentage error (GPE), maximum entropy (S(w)), maximum relative entropy ($S(w)/S_{max}$), maximum entropy-GPE ratio (S(w)/GPE)), distance (D), and its respective standard deviation (S). GCM had feasible solutions with some null weights, while NBI-MMSE had the highest S(w) (weight diversification) and did not prioritize some objective functions to the detriment of others. Desirability had the second largest weight diversification when initialized with a configuration obtained from NBI-MMSE points. However, NBI-MMSE had the smallest GPE and the largest S(w)/GPE with equal distances. NNC was competitive only when it adopted large weights for R_a function. Since desirability was tuned according to NBI-MMSE, only GCM was used without making reference to the correlation. However, this method had the greatest distance from the targets, with a GPE index of ~27.54%. Its S(w) was relatively small, with null weights

for several objectives and the least S(w)/GPE among the methods. Therefore, NBI-MMSE approach is best suited for optimizing correlated objective functions.

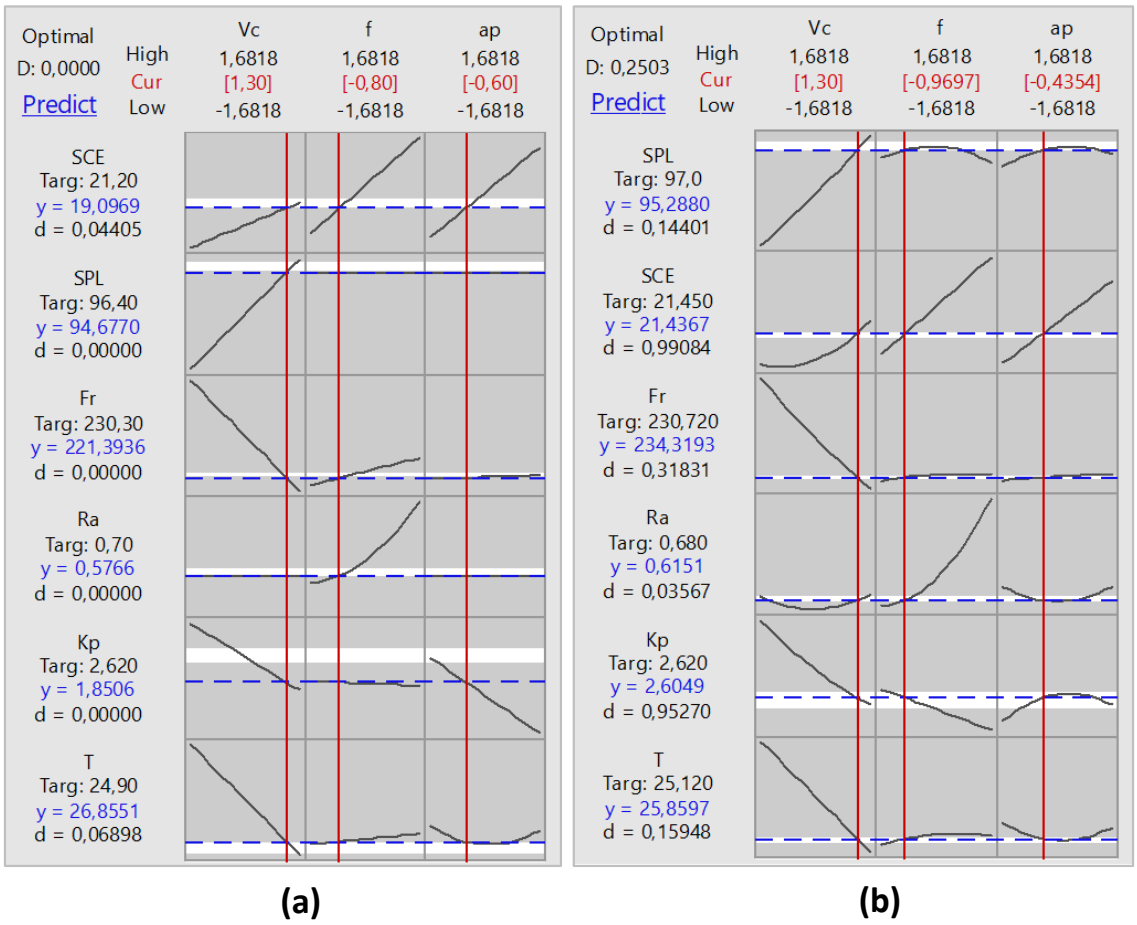

Figure 19: Desirability results (solutions guided by Pareto points of NBI-MMSE).

Fig. 20 illustrates the solution vectors as scatterplots. The points 1-6 represent the individual optimum (or Utopia points) of T, K_p, R_a, F_r, SPL and SCE respectively. Although most of the objective functions had high correlations, their individual optimum were not coincident and were sometimes too far apart. Hence, some individual solution were not gotten. However, some targets such as T, K_p and R_a were resized to avoid inconsistencies. These targets were not chosen based on the Utopia points of the payoff matrix but from the predicted values defined using partial least squares (PLS).

Points 3 and 7 (blue bullets) represent individual optimums of R_a and $MMSE_T$ respectively for the anchor points of NBI-MMSE. Point 8 (green bullet) represents the best Pareto solution, defined from the Pareto frontier of NBI-MMSE for w=0.8 (the maximal fuzzy decision membership) while points 9-12 represent solutions of the optimum of AHL, NNC, GCM, and desirability respectively.

Table 12. Comparisons among several multiobjective optimization methods.

MOP Method	**T**	**K_p**	**R_a**	**F_r**	**SPL**	**SCE**
NBI-MMSE	26.080	2.490	0.690	232.670	95.610	2.200
AHL	25.938	2.518	0.668	232.820	95.579	2.193
D	25.860	2.605	0.615	234.320	95.288	2.144
NNC	26.257	2.442	0.720	232.448	95.675	2.220
GCM	25.099	2.674	0.588	234.150	95.654	1.988
Target:	**24.900**	**2.620**	**0.700**	**230.300**	**96.390**	**2.120**
Weights	**w_1**	**w_2**	**w_3**	**w_4**	**w_5**	**w_6**
NBI-MMSE	0.1600	0.1600	0.2000	0.1600	0.1600	0.1600
AHL	0.0800	0.0800	0.6000	0.0800	0.0800	0.0800
D	0.1429	0.1429	0.2857	0.1429	0.1429	0.1429
NNC	0.0200	0.0200	0.9000	0.0200	0.0200	0.0200
GCM	0.6000	0.0000	0.0000	0.0000	0.0000	0.4000
Metrics:	**GPE**	**S(w)**	**S(w)/Smax**	**S(w)/GPE**	**D**	**S**
NBI-MMSE	16.74%	1.7880	0.9979	10.6799	0.0996	0.3285
AHL	18.08%	1.1600	0.6474	6.4163	0.0970	0.0000
D	20.58%	1.7479	0.9755	8.4930	-	-
NNC	21.54%	0.4860	0.2713	2.2564	0.0995	0.1076
GCM	27.54%	0.6730	0.3756	2.4440	-	-

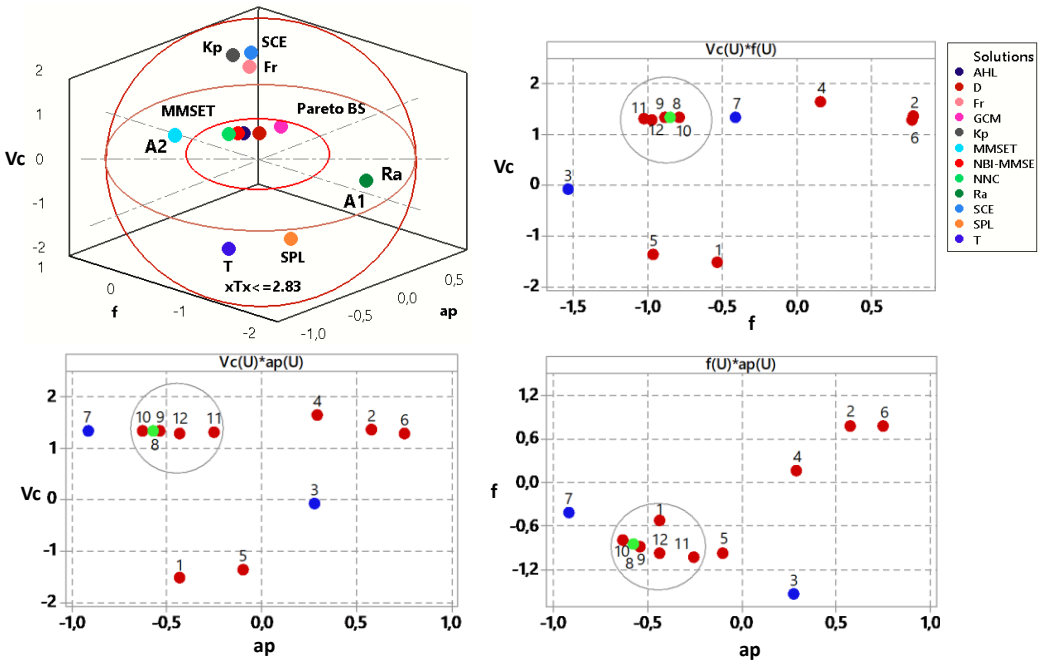

Figure 20: Spatial arrangement of the solutions within the sphere region. Utopia points (red bullets), Anchor points (blue bullets) and NBI-MMSE best point (Green).

One of the most intriguing patterns of non-compliance observed at Pareto frontiers of the response surfaces is the "inverted correlations paradigm" which was first observed by Lopes *et al*. (2016). It means that whenever two positively correlated functions are simultaneously minimized, the generated Pareto frontier will present the solutions with negative correlations

and different meanings from those presented by the real data. This generally happens because the weighted sums introduces complementary weights which leads to negatively-correlated relationships. This paradigm is observed in the Fig. 21.

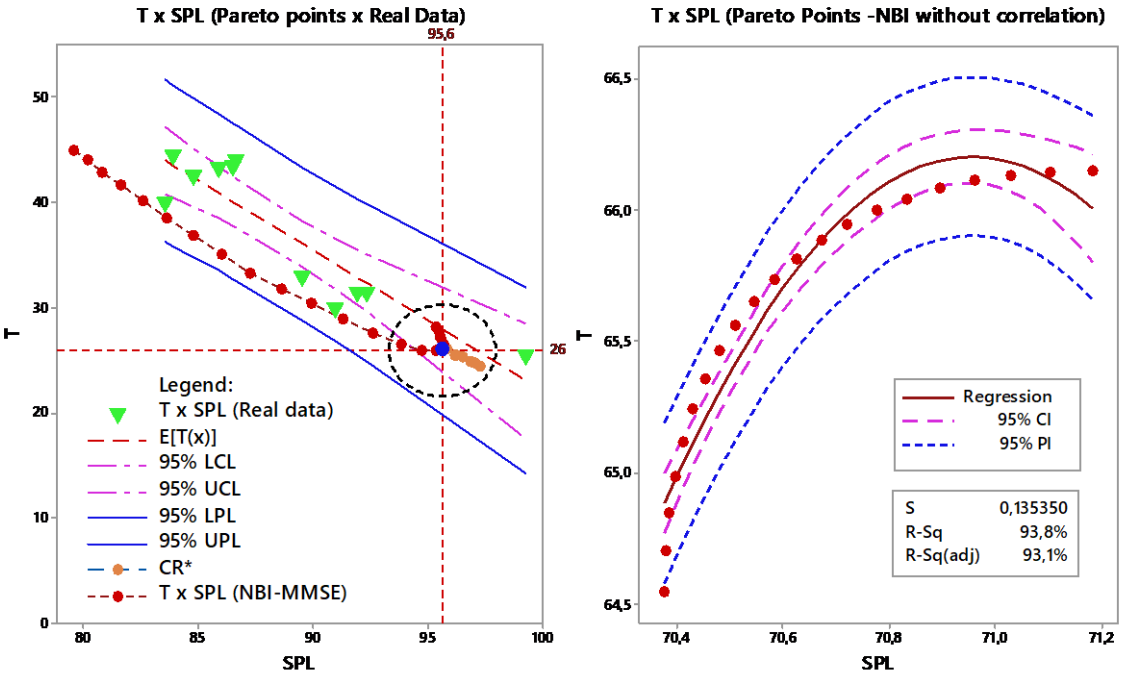

Figure 21: Pareto frontier of T versus SPL (Pearson correlation coefficient r=-0.921; P-Value=0.000).

The correlation between T and SPL were negative, significant (P-Value<5%), strong, and having a Pearson correlation coefficient of r=-0.921. When NBI-MMSE was used, the Pareto frontier followed the direction of the experimental data, with optimal values close to true relationship between the variables and to the confirmation runs. However, if NBI is applied directly to the negative correlated reponses, the Pareto points will show a positive (and false) correlation which is not compatible with the real data. The green, red, blue, and orange points represent the experimental data (from Table 2), NBI-MMSE Pareto frontier, best Pareto point, and confirmation runs respectively. If the correlations between the response surfaces are neglected, the Pareto frontier of the original data will fall outside confidence interval.

Generally, when optimization is applied to real-world engineering problems, confirmation tests and analyses should be done to verify whether the results are compatible with the phenomena under investigation or they are just mere numerical outcomes.

Although the results discussed above are specific to the AISI H13-PCBN 7025 hardened turning process, some aspects of the proposed methodology may find application in other areas. Therefore, we will use benchmark test functions to access its versatility in the next section.

6. Conclusion

This paper proposed an optimization method capable of identifying the optimal weights of a multiobjective problem. It caters for the complexity observed when multiple targets are significantly correlated.

Numerical results have shown that NBI-MMSE method surpassed other methods, with an optima of T=26 min, K_p=2.49 US$/piece, R_a=0.69 μm, F_r=232.6 N, SPL=95.6 dB, and SCE=2.22x10^{-2} cm^3/N.min for w=0.80. The best solution of the Pareto frontier was found using w=0.80 and with an optimum vector formed by a cutting speed (V_c) of 246.05 m/min, a feed rate (f) of 0.11 mm/rev, and a machining depth depth (A_p) of 0.19. Also, confirmation tests (n=10) were carried out using 10 different cutting edges machined up to the cutoff point of 0.3 mm of flank wear. There was no difference between mean of the experimental and mathematical vectors at α=5% significance level based on the multivariate confidence intervals. Hence,

- The analysis made by principal components allowed the use of only 2 responses with 21 problems;
- The correlations obtained among the six original responses were significant which allows for dimensionality reduction;
- The optimization results allowed the construction of a convex and equidistant Pareto frontier and the use of fuzzy decision maker to define the appropriate criteria for evaluating the solutions;
- The low values of total cost (K_p) and surface roughness (R_a) are significant in industrial applications. Given the increased environmental concerns regarding lubricant disposal, the ideal solution is clean as long as the use of refrigerant is not necessary for maintaining surface roughness at low levels, thereby lowering the cost of production;
- Tool wear is a natural consequence of the physical material removal process. Since tool performance diminishes with multiple machining passes, the optimal configuration was not able to ensure that the surface roughness values remain the same. Under ideal conditions, the tool life (T) lasts much longer and the quality of the machined surfaces is preserved in an ideal configuration. However, the tool life (T) is maximized by minimizing the machining force (F_r) and the sound pressure level (SPL), thereby reducing the cost of operation and improving the quality of the workpiece surface.

Therefore, the proposed method is able to identify the optimal solution within the limits specified for the machining process for the most efficient production. The method becomes

even more beneficial as the number of benchmark functions increases, since it permits a dimensionality reduction that leads to computational advantages. In addition, it does not reverse the correlation as opposed to the traditional NBI.

Acknowledgments

The authors express their gratitude to Prof. João Paulo Davim Tavares da Silva (PhD) of the University of Aveiro, Portugal, who allowed and sponsored the consecution of experimental data set. The authors also express their gratitude to the anonymous reviewers who greatly contributed to article´s improvement with a large deal of suggestions.

Funding: This work was supported by CAPES, Brazil (Fellow CAPES – grant number 9801-12.0), CNPq (grant number 303586/2015-0).

References

Aghaei, J., Amjady, N., and Shayanfar, H.A. 2011. Multi-objective electricity market clearing considering dynamic security by lexicographic optimization and augmented epsilon constraint method, Applied Soft Computing 11: 3846-3858.

Ahmadi, A., Aghaei, J., Shayanfar, H. A, and Rabiee, A. 2012. Mixed integer programming of multiobjectivehydro-thermal self scheduling, Applied Soft Computing 12: 2137-2146.

Ahmadi, A., Kaymanesh, A., Siano P., Janghorbani, M, Nezhad, A. E., and Sarno, D. 2015.Evaluating the effectiveness of normal boundary intersection method for short-term environmental/economic hydrothermal self-scheduling, Electric Power Systems Research 123: 192-204.

Ansoni, J. A., Seleghim Jr., P. 2016. Optimal industrial reactor design: development of a multiobjective optimization method based on a posteriori performance parameters calculated from CFD flow solutions, Advances in Engineering Software 91: 23-35.

Bouacha, K., Yallese, M. A., Mabrouki, T., Rigal J. F. 2010. Statistical analysis of surface roughness and cutting forces using response surface methodology in hard turning of AISI 52100 bearing steel with CBN tool, Int. J. Refract. Met. Hard Mater. 28: 349–361. doi:10.1016/j.ijrmhm.2009.11.011.

Box, G. E. P., Hunter, W. G., MacGregor, J. F., Erjavec, J. 1973. Some Problems Associated with the Analysis of Multiresponse Data. Technometrics, 15(1): pp. 33-51.

Brito, T. G., Paiva, A. P., Ferreira, J. R., Gomes, J. H. F., Balestrassi, P. P. 2014. A normal boundary intersection approach to multiresponse robust optimization of the surface roughness in end milling process with combined arrays. Precision Engineering, 38: 628–638.

Buczkowski, R., Kleiber, M. 2009. Statistical models of rough surfaces for finite element 3D-Contact analysis. Archives of Computational Methods in Engineering, 16: 399-424.

Campos, P.H.S. 2015. Metodologia DEA-OTS: Uma contribuição para a seleção ótima de ferramentas no Torneamento do Aço ABNT H13 Endurecido. Thesis, Federal University of Itajubá, Brazil.

Carvalho, L. A., Paiva, A. P., Leme, R. C., Costa, S. C., Aguiar, T. C. S. 2016. Optimization methodology of alternating current P-GMAW process by voltage-current signal analysis. Int. J. Adv. Manuf. Technol. 86.

doi:565–580 DOI 10.1007/s00170-015-8106-y

Costa, D. M. D., Brito, T. G., Paiva, A. P., Leme, R. C., Balestrassi, P. P. 2016. A normal boundary intersection with multivariate mean square error approach for dry end milling process optimization of the AISI 1045 steel. Journal of Cleaner Production. 135: 1658-1672.

Costa, D. M. D., Paula, T. I., Silva, P. A. P., Paiva, A. P. 2016. Normal boundary intersection method based on principal components and Taguchi's signal-to-noise ratio applied to the multiobjective optimization of 12L14 free machining steel turning process. Int. J. Adv. Manuf. Technol. 87: 825-834.

Das, I., and Dennis, J. E. 1998. Normal-Boundary Intersection: a new method for generating the Pareto surface in nonlinear multicriteria optimization problems, Society for Industrial and Applied Mathematics 8: 631–657. http://dx.doi.org/10.1137/S1052623496307510

Garg, A., Tai. K. 2014.Stepwise approach for the evolution of generalized genetic programming model in prediction of surface finish of the turning process. Advances in Engineering Software, 78: 16-27.

Gobbi, M., Guarneri, P., Scotti, L. S. L. 2014. A local approximation based multi-objective optimization algorithm with applications, Optim. Eng. 15:619–641. Doi: 10.1007/s11081-012-9211-5

Gomes, J. H. D. F., Paiva, A. P., Ferreira, J. R., Costa, S. C., Paiva, E. J. 2011. Modeling and Optimization of Multiple Characteristics in the AISI 52100 Hardened Steel Turning, Adv. Mater. Res. 223: 545–553. doi: 10.4028/www.scientific.net/AMR.223.545.

Haridy, S., Wu, Z., Castagliola, P. 2011. Univariate and multivariate approaches for evaluating the capability of dynamic-behavior processes (case study). Stat. Methodol. 8: 185–203. doi:10.1016/j.stamet.2010.09.003

He, Z., Han, Y. J., Zhao, S., Park, S. 2009. Product and process optimisation design through Design of Experiments: A case study. Total Quality Management & Business Excellence. 20(1): 107-113. doi: 10.1080/14783360802614315

Jamil, M., Yang, X. 2013. A literature survey of benchmark functions for global optimisation problems. Int. J. Mathematical Modelling and Numerical Optimisation. 4(2): 150-194.

Johnson, R. A., and Wichern, D. W. 2007. Applied Multivariate Statistical Analysis. 6ª ed, New Jersey: Pearson - Prentice Hall.

Kelesoglu, O. 2007. Fuzzy multiobjective optimization of truss-structures using genetic algorithm. Adances in Engineering Software 38: 717-721.

Kovach, J., and Cho, B. R. 2009. A D-optimal design approach to constrained multiresponse robust design with prioritized mean and variance considerations. Comput. Ind. Eng. 57: 237–245. doi:10.1016/j.cie.2008.11.011

Kumar, P., Chauhan, S. R. 2015. Machinability study on finish turning of AISI H13 hot working die tool steel with cubic boron nitride (CBN) cutting tool inserts using response surface methodology (RSM). Arab J Sci Eng. 40: 1471-1485. doi:10.1007/s13369-015-1606-0

Lin, S. H. I., Zhi-ling, L. I., Tao, Y. U., Jiang-peng, L. I. 2011. ScienceDirect Model of Hot Metal Silicon Content in Blast Furnace Based on Principal Component Analysis Application and Partial Least Square. J. Iron Steel Res. Int. 18: 13–16. doi:10.1016/S1006-706X(12)60015-6

Lin, W., Yu, D. Y., Wang, S., Zhang, C., Zhang, S., Tian, H., Luo, M., Liu, S. 2015. Multi-objective teaching-learning-based optimization algorithm for reducing carbon emissions and operation time in turning operations, Engineering Optimization 47: 994-1007. doi:10.1080/0305215X.2014.928818

Lopes, L. G. D., Brito, T. G., Paiva, A. P., Peruchi, R. S., Balestrassi, P. P. 2016. Robust parameter optimization

based on multivariate normal boundary intersection. Comput. Ind. Eng. 93: 55–66. doi:10.1016/j.cie.2015.12.023

Lopez, R. H., Ritto, T. G., Sampaio, R., Cursi, J. E. S. 2014. A new algorithm for the robust optimization of rotor-bearing systems. Eng. Optim. 46(8): 1123-1138. doi:10.1080/0305215X.2013.819095

Lu, L., Anderson-Cook, C. M., Robinson, T. J. 2011. Optimization of design experiments based on multiple criteria utilizing a Pareto Frontier. Technometrics. 53: 353-365. doi:10.1198/tech.2011.10087

Messac, A. , Ismail-Yahaya, A., Mattson, C. A. 2003. The normalized normal constraint method for generating the Pareto frontier. Struct Multidiscip Optim 25(2):86–98.

Messac, A., Mattson, C. A. 2002. Generating well-distributed sets of Pareto points for engineering design using physical programming. Optim. Eng. 3:431–450.

Messac, A., Mullur, A. A. 2008. A computationally efficient metamodeling approach for expensive multiobjective optimization, Optim Eng. 9: 37–67 DOI 10.1007/s11081-007-9008-0

Montgomery, D. C. 2012. Design and Analysis of Experiments. 8ª ed, New York: John Wiley.

Paiva, A. P., Paiva, E. J., Ferreira, J. R., Balestrassi, P. P., Costa, S. C. 2009. A multivariate mean square error optimization of AISI 52100 hardened steel turning. Int. J. Adv. Manuf. Technol. 43: 631–643. doi:10.1007/s00170-008-1745-5.

Paiva, A. P., Campos, P. H., Ferreira, J. R., Lopes, L. G. D., Paiva, E. J., Balestrassi, P. P. 2012. A multivariate robust parameter design approach for optimization of AISI 52100 hardened steel turning with wiper mixed ceramic tool. Int. J. Refract. Met. Hard Mater. 30: 152–163. doi:10.1016/j.ijrmhm.2011.08.001

Paiva, A. P., Gomes, J. H. F., Peruchi, R. S., Leme, R..C., Balestrassi, P.P. 2014. A multivariate robust parameter optimization approach based on Principal Component Analysis with combined arrays. Comput. Ind. Eng. 74: 186–198. doi:10.1016/j.cie.2014.05.018.

Pereira, R. B. D., Hincapie, C. A. A., Campos, P. H. S., Paiva, A. P., Ferreira, J. R. 2016. Multivariate global index and multivariate mean square error optimization of AISI 1045 end milling. Int. J. Adv. Manuf. Technol. 1–15. doi:10.1007/s00170-016-8703-4

Pereira, R. B. D., Leite, R. R., Alvim, A. C., Paiva, A. P., Balestrassi, P. P., Ferreira, J. R., Davim, J. P. 2017. Multivariate robust modeling and optimization of cutting forces of the helical milling process of the aluminum alloy Al 7075. Int. J. Adv. Manuf. Technol. 1–15. doi:10.1007/s00170-017-1398-3.

Pereyra, V., Saunders, M., Castillo, J. 2013. Equispaced Pareto front construction for constrained bi-objective optimization. Mathematical and Computer Modelling, 57: 2122-2131. Doi: 10.1016/j.mcm.2010.12.044.

Rao, J. S., and Tiwari, R. A. 2015. Pareto optimal design analysis of magnetic thrust bearings using multi-objective genetic algorithms. Int. J. Computational Methods in Eng. Science and Mechanics 16: 71-85. doi: 10.1080/0305215X.2014.928818

Rapcsák, T. 2004. Some optimization problems in multivariate statistics. Journal of Global Optimization 28: 217-228.

Rocha, L. C. S., Paiva, A. P., Balestrassi, P. P., Severino, G., Rotela Jr., P. 2015. Entropy-based weighting for multi-objective optimization: an application on vertical turning, Mathematical Problems in Engineering 2015. http://dx.doi.org/10.1155/2015/608325

Rocha, L. C. S., Paiva, A. P., Rotela Jr., P. Balestrassi, P. P., Campos, P. H. S. 2017. Robust multiple criteria decision making applied to optimization of AISI H13 hardened steel turning with PCBN wiper tool. Int J Adv

Mannuf Technol. 89: 2251-2268. doi:10.1007/s00170-016-9250-8

Rocha, L. C. S., Paiva, A. P., Paiva, E. J., P. Balestrassi, P. P. 2016. Comparing DEA and principal component analysis in the multiobjective optimization of P-GMAW process. J Braz. Soc. Mech. Sci. Eng. 38. doi:2513–2526 DOI 10.1007/s40430-015-0355-z.

Schatz, M. E., Hermanutz, A., Baier, H. J. 2017. Multi-criteria optimization of an aircraft propeller considering manufacturing: Structural design optimization simultaneously considering a knowledge-based manufacturing and a structural model, Struct Multidisc Optim. 55:899–911. Doi: 10.1007/s00158-016-1541-z.

Su, H., Luo, X. B., Chai, F., Shen, J. C., Sun, X. J., Lu, F. 2015. Manufacturing Technology and Application Trends of Titanium Clad Steel Plates, J. Iron Steel Res. Int. 22: 977–982. doi:10.1016/S1006-706X(15)30099-6

Umer, U., Qudeiri, J. A., Hussein, H. A. M., Khan, A. A., Al-ahmari, A. R. 2014. Multi-objective optimization of oblique turning operations using finite element model and genetic algorithm. Int J Adv Manuf Technol. 71: 593-603. doi: 10.1007/s00170-013-5503-y

Utyuzhnikov, S. V., Fantini, P., Guenov, M. D. 2009. A method for generating a well-distributed Pareto set in nonlinear multiobjective optimization. J. Comput. Appl. Math. 223: 820–841.

Xian, S., Qiu, D., Zhang, S. 2013. A Fuzzy Principal Component Analysis Approach to Hierarchical Evaluation Model for Balanced Supply Chain Scorecard Grading. J Optim Theory Appl 159: 518-535.

Yacoub, F., and MacGregor, J. F. 2004. Product optimization and control in the latent variable space of nonlinear PLS models. Chemom. Intell. Lab. Syst. 70: 63–74. doi:10.1016/j.chemolab.2003.10.004.

Zidani, H., Pgnacco, E., Sampaio, R., Ellaia, R., Cursi, J. E. C. 2013. Multi-objective optimization by a new hybridized method: appications to random mechanical systems. Engineering Optimization. 45(8): 917-939.

3. CONCLUSÃO

Esta seção possui o objetivo de descrever as conclusões obtidas em decorrência do desenvolvimento da pesquisa proposta e, bem como, mencionar as sugestões para trabalhos futuros. O uso de pares de estimadores robustos para modelar a rugosidade superficial (R_a) de um processo de torneamento do aço de corte fácil ABNT/SAE 12L14 foi apresentado.

Assim sendo, a Análise de Componentes Principais (ACP) foi aplicada e contextualizada na determinação das configurações dos parâmetros de entrada do processo objeto de estudo com o propósito de reduzir a dispersão da rugosidade superficial do corpo de prova e, assim, elevando o nível de qualidade do processo de torneamento. Juntamente, técnicas de otimização multivariada foram apresentadas e um sequenciamento de atividades.

Nesse sentido, foi proposto um algoritmo considerando funções objetivas em termos dos valores de MMSE e, em sequência, otimizadas pelo método NBI. A obtenção de soluções viáveis foi representada por uma fronteira de Pareto com definição do ponto ótimo por meio do tomador de decisão *fuzzy*. Essa decisão foi reforçada pelas elipses com 95% de confiança nos dados obtidos pelo experimento de confirmação.

Como resultado, foi determinado que o Modelo B compreendendo os estimadores não paramétricos como a mediana e o MAD, é o melhor. Consequentemente, o valor alvo obtido para R_a foi de 1,281 μm com um valor mínimo de dispersão de 0,555 μm. Esses valores foram obtidos considerando os seguintes parâmetros de entrada do processo: V_c = 273,853 [m/min], f = 0,084 [mm/rev] e d = 0,583 [mm].

Pensando na validação da resposta ótima obtida pelo algoritmo proposto, novos experimentos foram executados considerando os valores V_c = 280,00 [m/min], f = 0,10 [mm/rev] e d = 0,095 [mm] dos parâmetros de entrada da máquina. Desse modo, a rugosidade superficial do corpo de prova de ambos os experimentos foram comparadas através da microscopia eletrônica de varredura (MEV) comprovando que a rugosidade superficial obtida pelos parâmetros otimizados é menor. Este experimento foi desenvolvido no Laboratório de Caracterização Estrutural (LCE) da Universidade Federal de Itajubá (UNIFEI).

Por fim, também para fins de validação da resposta ótima obtida, foi realizada uma otimização multiobjetivo pelo algoritmo genético (função *gamultiobj*) nas 13 respostas originais modeladas pelos estimadores robustos. Desse modo, foi possível afirmar que as oito etapas apresentadas no algoritmo de otimização proporciona a construção de uma fronteira de

Pareto com soluções viáveis e não dominadas em relação às obtidas pelo algoritmo genético e, reafirmando assim, a eficiência das etapas de modelagem do algoritmo proposto.

Os demais artigos, publicado na *Engineering with Computers* e submetido na *Applied Soft Computing*, reforçam a validação do algoritmo de otimização proposto utilizando o agrupamento das respostas por meio da clusterização, a redução de dimensionalidade através da análise de componentes principais, a obtenção de funções objetivo em termos de MMSE, a otimização pelo método NBI e a obtenção do ponto ótimo, na fronteira de Pareto, pelo tomador de decisão *fuzzy*. O objeto de estudo utilizado foi o processo de torneamento do aço temperado AISI H13 considerando as ferramentas CC670 e PCBN 7025, respectivamente. Consequentemente, testes com demais métodos de otimização, além do NBI, foram realizados e, bem como, aplicações do algoritmo proposto em funções de teste também foram submetidas com o propósito de se verificar a eficiência do método em questão.

3.1 Contribuições da tese

Considerando os pontos apresentados anteriormente, as etapas de modelagem e, bem como, o algoritmo de otimização proposto; estes foram validados tanto em processos físicos quanto em funções de teste conhecidas. Ademais, a etapa de otimização proporcionou soluções viáveis por meio da fronteira de Pareto a qual foi comparada com os seguintes métodos de otimização: comprimento da homotopia de arco, critério global, somas ponderadas, restrição normal normalizada, critério global e *desirability*. Desse modo, conclui-se que:

- A otimização realizada entre funções correlacionadas nem sempre proporciona um conjunto de soluções Pareto-ótimas convexas e equiespaçadas;
- Quando o conjunto de respostas originais é modelado por componentes principais que eliminam a correlação entre as respostas, as soluções Pareto-ótimas tornam-se convexas e equiespaçadas e, assim, proporcionando o melhor conjunto de soluções ótimas que minimizam a dispersão dos dados e obtendo o valor alvo;
- A redução de dimensionalidade das respostas, a sua clusterização e a transformação em funções objetivo em termos da minimização do erro quadrático médio multivariado proporcionaram etapas de modelagem capazes de auxiliar na obtenção de soluções viáveis através de métodos de otimização conforme comprovado na comparação com o algoritmo genético;

- O método se torna mais vantajoso à medida que o número de funções aumenta, pois possibilita uma redução de dimensionalidade que leva a vantagens computacionais;
- A importância de uma análise de sensibilidade explícita é claramente enfatizada ao selecionar o número apropriado de saídas latentes para estabelecer uma fronteira de Pareto convexa, não dominada e equiespaçada;
- É possível definir qual par de estimadores é mais adequado para a modelagem de dados não paramétricos a serem analisados;
- O método proposto pode identificar a solução ótima dentro dos limites especificados do processo de usinagem obtendo a produção mais eficiente.

3.2 Sugestões para trabalhos futuros

Aspectos não abordados nesta tese devido às limitações previamente apresentadas podem ser considerados em trabalhos futuros com o propósito de evolução nos resultados. Tais sugestões estão descritas a seguir:

- Realizar a modelagem das respostas originais do processo objeto de estudo por meio de distribuições de probabilidade com o objetivo de modelar diferentes parâmetros de forma. Flutuações e variabilidade estão presentes na medição de valores durante a observação de um fenômeno e, desse modo, as distribuições de probabilidade podem modelar essas incertezas;
- Entender como a importância do autovalor atribuído ao componente principal impacta na fração do estimador na resposta otimizada;
- Além da obtenção do melhor par de estimadores, definir qual é a combinação ideal de estimadores capazes de modelar processos suscetíveis à presença de ruídos;
- Realizar demais comparações/simulações de cenários no processo experimental a fim de se testar a robustez dos pares de estimadores como considerar mais fatores de ruído no arranjo cruzado, elaborar experimentos por meio de um arranjo combinado, realizar mais réplicas experimentais ou oscilar os níveis de correlação entre as respostas coletadas;
- Considerar as incertezas (erros) existentes nas funções de teste utilizadas para validar o algoritmo de otimização proposto;

- Realizar a redução de dimensionalidade do problema através da análise fatorial e comparar se há melhora ou não na resposta ótima em relação à obtida pelos escores de componentes principais;
- Por fim, o método proposto pode ser estendido a outros processos de usinagem, de modo que as preocupações ambientais possam ser bem tratadas, juntamente com os objetivos de produtividade e qualidade.

REFERÊNCIAS BIBLIOGRÁFICAS

ARDAKANI, M. K.; NOOROSSANA, R. A new optimization criterion for robust parameter design — the case of target is best. **The International Journal of Advanced Manufacturing Technology**, v. 38, n. 9–10, p. 851–859, 2008.

BOYLAN, G. L.; CHO, B. R. Comparative studies on the high-variability embedded robust parameter design from the perspective of estimators. **Computers & Industrial Engineering**, v. 64, n. 1, p. 442–452, 2013.

DAS, I.; DENNIS, J. E. Normal-Boundary Intersection: a new method for generating the Pareto surface in nonlinear multicriteria optimization problems. **Society for Industrial and Applied Mathematics**, v. 8, n. 3, p. 631–657, 1998.

DUARTE COSTA, D. M.; BRITO, T. G.; DE PAIVA, A. P.; LEME, R. C.; BALESTRASSI, P. P. A normal boundary intersection with multivariate mean square error approach for dry end milling process optimization of the AISI 1045 steel. **Journal of Cleaner Production**, v. 135, p. 1658–1672, 2016.

ELSAYED, K.; LACOR, C. Robust parameter design optimization using Kriging, RBF, nad RBFNN with gradient-based and evolutionary optimization techniques. **Applied Mathematics and Computation**, v. 236, p. 325–344, 2014.

GAUDÊNCIO, J. H. D. **Influência dos estimadores robustos sobre a convexidade e equiespaçamento das Fronteiras de Pareto para problemas duais Influência dos estimadores robustos sobre a convexidade e equiespaçamento das Fronteiras de Pareto para problemas duais**. Universidade Federal de Itajubá (UNIFEI), 2015.

HAMPEL, F. R.; RONCHETTI, E. M.; ROUSSEEUW, P. J.; STAHEL, W. S. **Robust statistics - the approach based on influence functions**. John Wiley & Sons, 1986.

LOPES, L. G. D.; BRITO, T. G.; PAIVA, A. P. DE; PERUCHI, R. S.; BALESTRASSI, P. P. Robust parameter optimization based on multivariate normal boundary intersection. **Computers & Industrial Engineering**, v. 93, p. 55–66, 2016.

MESSAC, A.; ISMAIL-YAHAYA, A.; MATTSON, C. A. The normalized normal constraint method for generating the Pareto frontier. **Structural and Multidisciplinary Optimization**, v. 25 (2), p. 86–98, 2003.

PAIVA, A. P.; CAMPOS, P. H.; FERREIRA, J. R.; et al. A multivariate robust parameter design approach for optimization of AISI 52100 hardened steel turning with wiper mixed ceramic tool. **International Journal of Refractory Metals and Hard Materials**, v. 30, p. 152–163, 2012.

PARK, C.; CHO, B. R. DEVELOPMENT OF ROBUST DESIGN UNDER CONTAMINATED AND NON-NORMAL DATA. **Quality Engineering**, v. 15, n. 3, p. 463–469, 2003.

PEREIRA, V.; SAUNDERS, M.; CASTILLO, J. Equispaced Pareto front construction for constrained biobjective optimization. **Mathematical and Computer Modelling**, v. 57, p. 2122-2131, 2013.

SERFLING, R. Asymptotic Relative Efficiency in Estimation. **International encyclopedia of statistical sciences**, p. 68–72, 2011.

VINING, G. G.; MYERS, R. H. Combining Taguchi and Response Surface Philosophies: A dual response approach. **Journal of Quality Technology**, v. 22, n. 1, p. 38–45, 1990.

YOHAI, V. J.; ZAMAR, R. H. High breakdown-point estimates of regression by means of the minimization of an efficient scale. **Journal of the American Statistical Association**, v. 83, n. 402, p. 406–413, 1988.